Article

Journal of Vibration and Control
1–25

DOI: 10.1177/1077546315587611
jvc.sagepub.com
SAGE

Vibration mitigation of a rotating beam under external periodic force using a nonlinear energy sink (NES)

S Bab[1], SE Khadem[1], MK Mahdiabadi[2] and M Shahgholi[3]

Abstract

In this paper, the performance of a smooth nonlinear energy sink (NES) to mitigate vibration of a rotating beam under an external force is investigated. The rotating beam is modeled using the Euler-Bernoulli beam theory, and the centrifugal stiffening effect is considered. It is assumed that the nonlinear energy sink has a linear damping and an essentially nonlinear (nonlinearizable or cubic) stiffness. Required conditions for occurring Hopf bifurcation, saddle-node bifurcation and strongly modulated responses (SMR) in the system are investigated. The most important parameter to study NES performance is SMR occurrence range in the detuning parameter span. Effects of position and damping of the NES and magnitude of the external force on the vibration mitigation of the rotating beam are studied. The Complexification-Averaging and the Runge Kutta methods are employed for analytical and numerical investigations, respectively. Finally, the efficiency of an optimal linear absorber and an optimal NES in the vibration mitigation of the rotating beam are compared. It is shown that the best range for the parameters of the NES is the one in which SMR and weak modulated response occur simultaneously. Furthermore, the best position for connecting the NES to a rotating beam is at the beam tip.

Keywords

Rotating beam, smooth nonlinear energy sink, saddle-node bifurcation, hopf bifurcation, strongly modulated response (SMR), weakly modulated response (WMR)

1. Introduction

Since many industrial structures such as gas turbine, helicopter and windmill turbine blades are modeled as rotating beams, the vibration analysis of the rotating beam is an interesting research area. Vibration of the rotating beam is more complex in comparison to a non-rotating beam. It is influenced by different factors such as the centrifugal force and various external excitations. The 'engine order excitation' is one of these forces that is very important in the turbo-machinery context. Due to the importance of this vibration and the risk of failure of equipments resulted by it, the rotating beam vibration mitigation is an important issue in the literature.

Sanches et al. (2011) investigated a helicopter ground resonance in isotropic and anisotropic multi-bladed rotor configurations. They used Floquet theory for the nonlinear dynamic analysis of the system. In addition, the system bifurcation points, which depend on the anisotropic parameters, were determined.

Dai et al. (2001) examined a rotor-bearing system with the magnetic bearings, hydrodynamic bearings and squeeze film dampers. Using a four-degree of freedom model, the linear dynamic of the system was described. The unbalance response of the system was investigated. They demonstrated that squeeze film damper significantly decreases the amplitude of

[1]Department of Mechanical Engineering, Tarbiat Modares University, Tehran, Iran
[2]Technische Universität München, Fakultät für Maschinenwesen, Institute for Applied Mechanics, Garching, Germany
[3]Shahid Rajaee Teacher Training University, Tehran, Iran

Received: 1 June 2014; accepted: 26 April 2015

Corresponding author:
SE Khadem, Department of Mechanical Engineering, Tarbiat Modares University, PO Box 14115-177, Tehran, Iran.
Email: Khadem@modares.ac.ir

vibrations and unstable region of dynamic behavior of the system.

Duffy et al. (2000, 2004) analyzed the influence of a self-tuning impact damper on the vibration attenuation of rotating components of turbo-machinery. The numerical and experimental results showed that self-tuning impact damper decreases vibration amplitude and hence, it increases the fatigue life of the components.

Byers and Gandhi (2009) studied the dynamic effects of two vibration absorbers in the radial and chordwise directions embedded in the helicopter blades. The blade and absorbers were modeled as a discrete two-degree of freedom system. Analytical results showed that the radial absorber in compare with chordwise absorber has a more efficient performance on the vibration reduction of the helicopter blades.

Gerges and Vickery (2003) considered the efficiency of a nonlinear tuned mass damper (TMD) on the vibration mitigation of a slender structure with square cross-section. A wire rope spring was used as a nonlinear TMD. The results of numerical and analytical analyses were validated by a wind tunnel test.

In recent years, nonlinear energy sink (NES) is widely taken into consideration for vibration mitigation of discrete and continuous systems, instead of tuned mass damper (TMD) or weakly nonlinear absorber.

Ahmadabadi and Khadem (2012a) investigated attenuation of a drill string self excited oscillations, using a nonlinear energy sink. Various positions of the drill string for attaching of the NES was examined. They showed that nonlinear energy sink decreases the drill string vibrations.

Samani and Pellicano (2009) studied the effects of linear and nonlinear absorbers on the vibration annihilation of a simply supported beam stimulated by a moving load. Two criterions of the maximum vibration amplitude and portion of dissipated energy of the system by the absorbers were used to study the efficiency of the absorbers. Furthermore, the optimal position of the absorbers on the beam was determined.

Grinberg et al. (2012) examined the vibration attenuation of a single-degree of freedom oscillator subjected to a harmonic force using a two-degree of freedom NES. Periodic, quasi-periodic and chaotic responses were observed in the dynamic regimes of the system. They showed that two-degree of freedom (2DOF) NES in compare with single-degree of freedom (SDOF) NES in a greater range of the amplitude of external force has a higher efficiency. The analytical results have a good agreement with numerical ones.

Lamarque and Savadkoohi (2014a) studied the multi-scale energy interchange between a main oscillator of Bouc–Wen type and a nonlinear energy sink. They acquired the invariant manifold in fast time scale, and equilibrium points and fold singularities in the slow time scale. Using numerical example, performance of the nonlinear energy sink for vibration mitigation of the Bouc–Wen type main structures was confirmed. Likewise, Lamarque and Savadkoohi (in press) and Weiss et al. (2014), investigated the efficiency of the nonlinear energy sink on the vibration mitigation of the system with a set of Saint-Venant elements. Domany and Gendelman (2013) studied dynamics of Van der Pol–Duffing (VdPD) oscillator with attached nonlinear energy sink. They illustrated that the dynamics of the system were described using a combination of averaging and multiple scales methods. It was shown that the nonlinear energy sink efficiently attenuate the undesired LCOs in the system response.

Ahmadabadi and Khadem (2012b) studied vibration mitigation of a two-degree of freedom system using an NES with nonlinear damping. They tuned NES parameters, in order to attenuate vibration perfectly, and to have a maximum strongly modulated responses (SMR) region in the vicinity of both modes of the primary system, simultaneously. Ahmadabadi and Khadem (2014) studied a coupled nonlinear energy sink (NES) and a piezoelectric-based vibration energy harvester positioned on a free-free beam under a shock excitation. The efficiency of the NES and the Harvester for two configurations were investigated, and hence, the optimal parameters of the system for the maximum dissipated energy in the NES, and the highest energy harvesting by piezoelectric element were extracted. Bab et al. (2014) investigated the performance of a number of smooth nonlinear energy sinks (NESs) on the vibration attenuation of a rotor system under mass eccentricity force. The nonlinear energy sinks had a linear damping, linear stiffness and a cubic stiffness. They utilized Jeffcott model for modeling of the rotor and derived the equations of the motion employing the Lagrange method. For analytical solution, Multiple Scales-Harmonic Balance Method (MSHBM) was used. It was demonstrated that, when the external force reaches its medium magnitude, the range of happening of SMR in the area of the system parameters get wider and the collection of the NESs illustrate a drastic effect.

Georgiades and Vakakis (2009) studied nonlinear interaction between different types of an NES and a thin cantilever plate on an elastic foundation. Attachment of the SDOF NES, two SDOF NESs at two different positions, and a multi-degree of freedom (MDOF) NES to the plate are considered and the behavior of the system in these configurations was examined. They demonstrated that the best locations for the attachment of NES to the plate are the antinodes of the plate. Georgiades and Vakakis (2007) investigated the nonlinear phenomena due to an NES

which is attached to a simply supported beam under a shock excitation. They showed numerically that the energy transfer approximately occurred in one direction from the beam to NES in this system. Georgiades et al. (2007) examined interaction between a rod and an NES. The nonlinear energy sink was attached to the rod free end. The transient nonlinear dynamic in the coupled NES and rod system subjected to a shock pulse was investigated. The optimum parameters for efficient targeted energy transfer were extracted using the Wavelet, Empirical Mode Decomposition and Hilbert transforms.

Ahmadabadi and Khadem (2012c) reviewed the influence of grounded and ungrounded nonlinear energy sink attached to a cantilever beam on the energy mitigation of the coupled system under an external shock. They investigated the effect of the nonlinear normal modes of the system on the occurrence of one-way irreversible energy pumping. Mehmood et al. (2014) surveyed usefulness of a nonlinear energy sink (NES) on the passive control of the vortex-induced vibrations of a freely oscillating circular cylinder. The flow pressure on the cylinder was extracted employing a direct numerical simulation of the incompressible flow over the cylinder. They showed that by changing mass ratio of the NES to the primary system and damping, the primary system had various behavior. They depicted that, depending on initial conditions, this system had multiple stable responses.

Luongo and Zulli (2012) introduced a general solution for evaluation of the performance of an essentially nonlinear oscillator with small mass and damping (NES), which was attached to a general, nonlinear, MDOF system, motivated by harmonic external force. They applied Multiple Scale-Harmonic Balance Method (MSHBM) to study dynamic of the system analytically. The main superiority of the method was that no complexification-averaging is required, and therefore, the analyses were performed using the classical perturbation techniques. Luongo and Zulli (2013) studied the performance of the nonlinear energy sinks on the controlling of aeroelastic instability of a two-degree-of-freedom rigid airfoil under steady wind. They employed the MSHBM method for analytical solution and obtained results were compared with numerical results. Also, Zulli and Luongo (2014) investigated the performance of the nonlinear energy sink on the vibration mitigation of an internally nonresonant elastic string using the MSHBM method.

Gendelman (2011) presented efficiency of the NES on the absorbing and suppressing broadband initial excitations of different primary system. It was shown that using NESs is a possible engineering solution for more traditional problems of vibration mitigation such as self-excited attenuation and externally forced systems under single or multiple frequency excitation. Vaurigaud et al. (2013) studied dynamic behavior of a system which composed of a two degree of freedom suspension bridge model and a single degree of freedom NES. The dynamic behavior was considered in a 1:1:1 nonlinear resonance condition. They used the complexification methods, multiple scales expansions and the concept of limiting phase trajectories (LPTs) for analytical analysis. Optimal parameters of the NES for efficient vibration reduction were obtained. Their numerical results had a good agreement with analytical predictions.

According to the above works, one distinguishes that survey of effects of the smooth NES on vibration attenuation of a rotating beam under an external force promises interesting results. In this paper, the Euler-Bernoulli beam theory is used to model the rotating beam where the centrifugal stiffening effect is considered. The source of the external force at the end of the rotating beam is due to the variation of the gas stream pressure passing through blades that is known as 'engine order excitation'. The NES has a small mass and damping. Also, the damping of the NES is linear, but its stiffness is nonlinearizable. In the presence of SMR in the system, the absorber has an optimum attenuating effect (Gendelman et al., 2008; Starosvetsky and Gendelman, 2008a). In order to detect the best efficiency of the absorber, attachment of the NES to various points of the rotating beam is considered. Furthermore, the existence of the saddle-node bifurcation, Hopf bifurcation and SMR in the F and α space are investigated. Occurrence of the Hopf bifurcation is the sign of a weak modulated response (WMR) happening in the system. In addition, the frequency response curves of the system are depicted. The most important parameter for study of the NES performance is occurrence of the SMR behavior in the detuning parameter range. Also, the effects of absorber position and external force magnitude on vibration attenuation of the rotating beam are studied. Finally, the optimal parameters of the NES for maximum performance in the vibration mitigation are determined.

2. Equations of motion

Figure 1 represents a rotating beam with an attached NES where its free end is under periodic external force. Indeed, the rotating beam is a simple model of a Turbomachinery blades. The most important periodic force, which is applied to the turbomachinery blades, is known as 'engine order excitation'. This force is due to the variable gas stream pressure passing through the blades. This issue has various reasons from the engine design and operation viewpoint (Ewins, 2010). The coupled equations of motion of the rotating

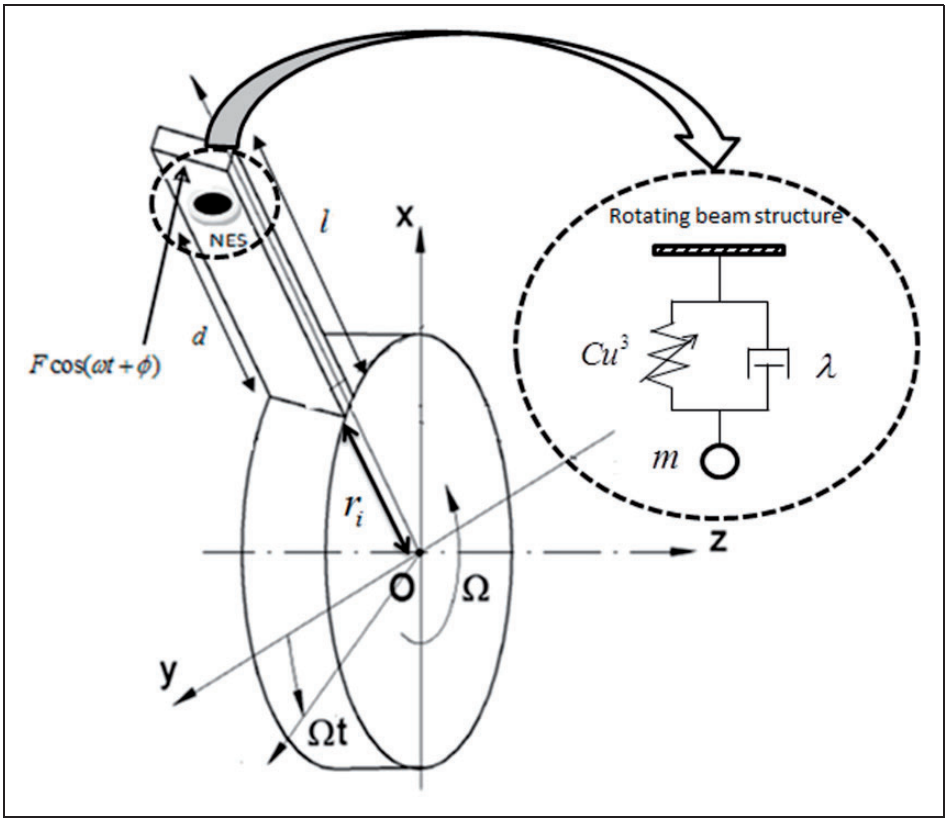

Figure 1. The rotating beam to which NES is attached.

beam and the attached NES under the periodic external force are governed by considering the centrifugal stiffening effect (Genta, 2005)

$$\begin{aligned}
&\rho A\frac{\partial^2 v(r,t)}{\partial t^2}-\rho A\Omega^2 v(r,t)+\rho A\Omega^2 r\frac{\partial v(r,t)}{\partial r}\\
&\quad-\rho A\frac{\Omega^2}{2}(r_0^2-r^2)\frac{\partial^2 v(r,t)}{\partial r^2}+EI\frac{\partial^4 v(r,t)}{\partial r^4}\\
&\quad+\left\{C[v(r,t)-u(t)]^3+\lambda\left[\frac{\partial v(r,t)}{\partial t}-\frac{\partial u(t)}{\partial t}\right]\right\}\\
&\quad\times\delta(r-(r_i+d))\\
&=F\cos(\omega t+\phi)\delta(r-(r_i+l))\quad r_i<r<r_i+l,\\
&m\frac{\partial^2 u(t)}{\partial t^2}+C[u(t)-v(r_i+d,t)]^3\\
&\quad+\lambda\left[\frac{\partial u(t)}{\partial t}-\frac{\partial v(r_i+d,t)}{\partial t}\right]=0
\end{aligned}\tag{1}$$

It is obvious that in this case the rotating beam is a clamped-free beam. Here $u(t)$ and $v(r,t)$ are displacements of the NES and the rotating beam, respectively. m, C and λ are the mass, nonlinearizable stiffness and damping of the NES, respectively. d represents the distance of the NES from the base of the beam. ρ, A, l, r_i and r_0 are the mass density, cross sectional area, length, inner radius and outer radius of the rotating beam, respectively. Ω is an angular velocity of the rotating beam. F and ω are amplitude and angular frequency of the external force. The rotating beam is modeled using Euler-Bernoulli beam theory and the centrifugal stiffening effect is considered.

For the sake of simplicity, the following dimensionless parameters are defined

$$\begin{aligned}
&\bar{v}=v/l,\quad \bar{r}=r/l,\quad \bar{t}=t/z,\\
&\bar{\Omega}=z\Omega,\quad \bar{r}_0=r_0/l,\quad \bar{r}_i=r_i/l,\\
&\bar{u}=u/l,\quad \bar{d}=d/l,\quad \gamma=\rho Al^4\Omega^2/EI,\quad \varepsilon=m/\rho Al,\\
&\bar{\omega}=\omega z,\quad \beta=\rho ACl^6/mEI,\quad \alpha=\lambda l^2/m\sqrt{\rho A/EI},\\
&\bar{F}=\rho AFl^4/mEI,\quad z=\sqrt{\rho Al^4/EI}
\end{aligned}\tag{2}$$

Using these dimensionless parameters, the following dimensionless equations of motion are obtained

$$\frac{\partial^2\bar{v}(\bar{r},\bar{t})}{\partial\bar{t}^2}-\bar{\Omega}^2\bar{v}(\bar{r},\bar{t})+\bar{\Omega}^2\bar{r}\frac{\partial\bar{v}(\bar{r},\bar{t})}{\partial\bar{r}}-\frac{\bar{\Omega}^2}{2}(\bar{r}_0^2-\bar{r}^2)\frac{\partial^2\bar{v}(\bar{r},\bar{t})}{\partial\bar{r}^2}$$

$$+\frac{\partial^4 \bar{v}(\bar{r},\bar{t})}{\partial \bar{r}^4}+\left\{\varepsilon\beta[\bar{v}(\bar{d},\bar{t})-\bar{u}(\bar{t})]^3+\varepsilon\alpha\left[\frac{\partial \bar{v}(\bar{d},\bar{t})}{\partial \bar{t}}-\frac{\partial \bar{u}(\bar{t})}{\partial \bar{t}}\right]\right\}$$
$$\times\delta(\bar{r}-(\bar{r}_i+\bar{d}))$$
$$=\varepsilon\bar{F}\cos(\bar{\omega}\bar{t}+\phi)\delta(\bar{r}-(\bar{r}_i+1)) \quad \bar{r}_i<\bar{r}<\bar{r}_i+1,$$
$$\varepsilon\frac{\partial^2 \bar{u}(\bar{t})}{\partial \bar{t}^2}+\varepsilon\alpha\left[\frac{\partial \bar{u}(\bar{t})}{\partial \bar{t}}-\frac{\partial \bar{v}(\bar{d},\bar{t})}{\partial \bar{t}}\right]+\varepsilon\beta[\bar{u}(\bar{t})-\bar{v}(\bar{d},\bar{t})]^3=0 \quad (3)$$

Using the Galerkin method, an approximate solution of the rotating beam displacement is supposed to be as $\bar{v}(\bar{r},t)=\sum_{j=1}^{n}\phi_j(\bar{r})q_j(\bar{t})$. where $\phi_j(\bar{r})$ is the linear mode shape of the undamped rotating beam. Since, the rotating beam is clamped-free, the linear mode shape of the clamped-free beam is used (Meirovitch, 2001). Using the first mode of the cantilever beam ($\phi_1(\bar{r})$) in the Galerkin method, the following coupled equations of the NES and rotating beam are obtained

$$m_{11}\ddot{q}_1(\bar{t})+k_{11}q_1(\bar{t})+\varepsilon\alpha\phi_1(\bar{r}_i+\bar{d})\{\phi_1(\bar{r}_i+\bar{d})\dot{q}_1(\bar{t})-\dot{\bar{u}}(\bar{t})\}+\varepsilon\beta\phi_1(\bar{r}_i+\bar{d})\{\phi_1(\bar{r}_i+\bar{d})q_1(\bar{t})-\bar{u}(\bar{t})\}^3$$
$$=\varepsilon\bar{F}\phi_1(\bar{r}_i+1)\cos(\bar{\omega}\bar{t}+\phi),$$
$$\varepsilon\ddot{\bar{u}}(\bar{t})+\varepsilon\alpha[\dot{\bar{u}}(\bar{t})-\phi_1(\bar{r}_i+\bar{d})\dot{q}_1(\bar{t})]+\varepsilon\beta[\bar{u}(\bar{t})-\phi_1(\bar{r}_i+\bar{d})q_1(\bar{t})]^3=0 \quad (4)$$

m_{11} and k_{11} are presented in Appendix A. Starosvetsky and Gendelman (2008b) showed that in the system under periodic or narrowband excitation (not impact, transient or wide-band excitations), when the frequencies of the primary system are well separated, the system can be considered as a two-degree of freedom system, which includes the desired mode of the primary system and NES. Since the natural frequencies of the rotating beam which is considered, are quite separated from each other, the coupled rotating beam and NES system can be considered as a two-degree of freedom system, which includes the first (and the most important) mode of the rotating beam and NES. The coefficients of the equation (4) are functions of the physical and geometrical parameters of the system, which are presented in Appendix A. To simplify the equation (4), the following transformation is introduced as $q'_1(\bar{t})=\phi_1(\bar{r}_i+\bar{d})q_1(\bar{t})$. In this relation, $q_1(\bar{t})$ and $q'_1(\bar{t})$ are the displacements of the first mode of the rotating beam and the rotating beam at the NES position, respectively. By introducing this relation into equation (4), and using these simplifications $\phi_1(\bar{r}_i+\bar{d})=\phi_{1d}$, $\phi_1(\bar{r}_i+1)=\phi_{1o}$, $m'_{11}=m_{11}/\phi_{1d}^2$, $k'_{11}=k_{11}/\phi_{1d}^2$ and $\phi'_{1o}=\phi_{1o}/\phi_{1d}$, the following equations are obtained

$$m'_{11}\ddot{q}'_1(\bar{t})+k'_{11}q'_1(\bar{t})+\varepsilon\alpha\{\dot{q}'_1(\bar{t})-\dot{\bar{u}}(\bar{t})\}+\varepsilon\beta\{q'_1(\bar{t})-\bar{u}(\bar{t})\}^3=\varepsilon\bar{F}\phi'_{1o}\cos(\bar{\omega}\bar{t}+\phi),$$
$$\varepsilon\ddot{\bar{u}}(\bar{t})+\varepsilon\alpha[\dot{\bar{u}}(\bar{t})-\dot{q}'_1(\bar{t})]+\varepsilon\beta[\bar{u}(\bar{t})-q'_1(\bar{t})]^3=0 \quad (5)$$

These equations demonstrate the dynamic behavior of the coupled rotating beam-NES system.

3. Analytical solution

3.1. Stability and bifurcation analysis

The dynamic behavior of the steady-state responses of the coupled beam and NES system is analyzed using the Complexification-Averaging method. This method was developed by Manevitch for extraction of transient and steady state response of a systems with nonlinear energy sink (Manevitch, 2001; Manevitch and Manevitch, 2005). Some usage of the Complexification-Averaging could be seen in (Lee et al., 2006, 2007). The motion of the system can be separated into two parts: the fast-varying and slow-varying motions. The fast and slow parts are related to the natural frequency and amplitude of the vibration, respectively.

To analyze the behavior of the system around 1:1 resonance of the first natural frequency of the rotating beam ($\omega_1=\sqrt{k'_{11}/m'_{11}}$), it can be considered ($\omega_1=\bar{\omega}+\varepsilon\eta$). Therefore, ($\omega_1^2=\bar{\omega}^2+\varepsilon^2\eta^2+2\varepsilon\eta\bar{\omega}$) and by refraining from higher order of ε and assuming $\sigma=2\varepsilon\eta$, it is obtained that ($\omega_1^2=\bar{\omega}^2+\varepsilon\sigma$) or $k'_{11}=m'_{11}(\bar{\omega}^2+\varepsilon\sigma)$. Consequently, the following equations of motion are obtained

$$m'_{11}\ddot{q}'_1(\bar{t})+m'_{11}(\bar{\omega}^2+\varepsilon\sigma)q'_1(\bar{t})+\varepsilon\alpha\{\dot{q}'_1(\bar{t})-\dot{\bar{u}}(\bar{t})\}+\varepsilon\beta\{q'_1(\bar{t})-\bar{u}(\bar{t})\}^3-\varepsilon\bar{F}\phi'_{1o}\cos(\bar{\omega}\bar{t}+\phi)=0$$
$$\varepsilon\ddot{\bar{u}}(\bar{t})+\varepsilon\alpha[\dot{\bar{u}}(\bar{t})-\dot{q}'_1(\bar{t})]+\varepsilon\beta[\bar{u}(\bar{t})-q'_1(\bar{t})]^3=0 \quad (6)$$

To analyze the effect of the NES on the system behavior, a transformation is defined as

$$v(t)=q'_1(\bar{t})+\varepsilon\bar{u}(\bar{t}), \quad w(t)=q'_1(\bar{t})-\bar{u}(\bar{t}) \quad (7)$$

For the sake of simplicity, the prim and bar marks are omitted in the following equations. Here, $v(t)$ is the deflection of center of mass of the beam and NES, and $w(t)$ is the NES displacement relative to the beam. In the averaging method, the response of the system is obtained using the sum of the responses of dominant frequencies. Here, it can be assumed that the system has one dominant frequency. Accordingly, it can be written as $v(t)=v_1(t)$, $w(t)=w_1(t)$. According to the Complexification Averaging method, the following complex parameters are introduced (Manevitch, 2001)

$$\psi_1(t)=\frac{dv_1(t)}{dt}+i\bar{\omega}v_1(t),$$
$$\psi_2(t)=\frac{dw_1(t)}{dt}+i\bar{\omega}w_1(t) \quad (8)$$

where $i^2 = -1$. The spatial variables and their derivatives in equation (8), in terms of the new complex variables, are obtained as

$$\begin{aligned} v_1(t) &= \frac{\left(\psi_1(t) - \overline{\psi_1(t)}\right)}{2i\bar{\omega}}, \\ w_1(t) &= \frac{\left(\psi_2(t) - \overline{\psi_2(t)}\right)}{2i\bar{\omega}}, \\ \frac{dv_1(t)}{dt} &= \frac{\left(\psi_1(t) + \overline{\psi_1(t)}\right)}{2}, \\ \frac{dw_1(t)}{dt} &= \frac{\left(\psi_2(t) + \overline{\psi_2(t)}\right)}{2}, \\ \frac{d^2v_1(t)}{dt^2} &= \frac{\mathrm{d}\psi_1(t)}{dt} - \frac{i\bar{\omega}}{2}\left(\psi_1(t) + \overline{\psi_1(t)}\right), \\ \frac{d^2w_1(t)}{dt^2} &= \frac{\mathrm{d}\psi_2(t)}{dt} - \frac{i\bar{\omega}}{2}\left(\psi_2(t) + \overline{\psi_2(t)}\right) \end{aligned} \tag{9}$$

The fast and slow parts of the motion are obtained by dividing the complex responses into two parts as

$$\begin{aligned} \psi_1(t) &= \phi_1(t)\mathrm{e}^{i\bar{\omega}t}, \quad \overline{\psi_1(t)} = \overline{\phi_1(t)}\mathrm{e}^{-i\bar{\omega}t}, \\ \psi_2(t) &= \phi_2(t)\mathrm{e}^{i\bar{\omega}t}, \quad \overline{\psi_2(t)} = \overline{\phi_2(t)}\mathrm{e}^{-i\bar{\omega}t} \end{aligned} \tag{10}$$

Here $(\mathrm{e}^{i\omega_0 t})$ shows the fast-varying part of the dynamic of the system (the vibration frequency), and $\phi_k(t)$, $k = 1, 2$ indicates the slow-varying, complex-valued amplitude modulations (the vibration amplitudes). Substituting equations (7) thorough (10) into equation (6), the ordinary differential equations of the slow motion are governed by

$$\begin{aligned} &\frac{d\phi_1(t)}{dt} - \frac{1}{8\bar{\omega}^3(1+\varepsilon)}\Big\{\varepsilon\{3i\varepsilon\beta\phi_2(t)\left|\phi_2(t)\right|^2\phi_{1d}^2 \\ &- 4\varepsilon\alpha\phi_{1d}^2\bar{\omega}^3\phi_2(t) + 4F\phi_{1o}\varepsilon\phi_{1d}^2\bar{\omega}^3 \\ &+ 4i\sigma\phi_1(t)\bar{\omega}^2 - 4\alpha\phi_2(t)\bar{\omega}^3\phi_{1d}^2 \\ &+ 4i\varepsilon\sigma\phi_2(t)\bar{\omega}^2 + 4F\phi_{1o}\bar{\omega}^3\phi_{1d}^2 + 3i\beta\phi_2(t)\left|\phi_2(t)\right|^2 \\ &\times \phi_{1d}^2 + 4\alpha\phi_2(t)\bar{\omega}^3 - 3i\beta\phi_2(t)\left|\phi_2(t)\right|^2 \\ &+ 4\alpha\bar{\omega}^3\varepsilon\phi_2(t) - 3i\varepsilon\beta\phi_2(t)\left|\phi_2(t)\right|^2 \\ &+ 4i\bar{\omega}^2\phi_2(t) - 4i\bar{\omega}^4\phi_1(t)\}\Big\} = 0 \\ &\frac{d\phi_2(t)}{dt} - \frac{1}{8\bar{\omega}^3(1+\varepsilon)}\Big\{3i\varepsilon^2\beta\phi_2(t)\left|\phi_2(t)\right|^2\phi_{1d}^2 \\ &- 4\varepsilon^2\alpha\phi_{1d}^2\bar{\omega}^3\phi_2(t) + 4F\phi_{1o}\varepsilon^2\phi_{1d}^2\bar{\omega}^3 \\ &+ 4i\bar{\omega}^2\varepsilon\sigma\phi_1(t) - 4\varepsilon\alpha\phi_{1d}^2\bar{\omega}^2\phi_2(t) \\ &+ 4i\bar{\omega}^2\varepsilon^2\sigma\phi_2(t) + 4F\phi_{1o}\varepsilon\phi_{1d}^2\bar{\omega}^3 \\ &+ 3i\varepsilon\beta\phi_2(t)\left|\phi_2(t)\right|^2\phi_{1d}^2 - 4\alpha\bar{\omega}^3\varepsilon\phi_2(t) \\ &+ 3i\varepsilon\beta\phi_2(t)\left|\phi_2(t)\right|^2\phi_{1d}^2 - 4\alpha\bar{\omega}^3\varepsilon\phi_2(t) \\ &+ 3i\varepsilon\beta\phi_2(t)\left|\phi_2(t)\right|^2 + 3i\beta\phi_2(t)\left|\phi_2(t)\right|^2 \\ &- 4\alpha\bar{\omega}^3\phi_2(t) - 4i\bar{\omega}^4\phi_2(t) + 4i\bar{\omega}^4\phi_1(t)\Big\} = 0 \end{aligned} \tag{11}$$

To obtain the steady sate responses of the system, the derivative with respect to the time of the slow varying modulation in equation (11) should be equal to zero ($\frac{d\phi_1(t)}{dt} = 0$, $\frac{d\phi_2(t)}{dt} = 0$). Then, by introducing $\phi_1(t)$ from the first relation of equation (11) and substituting it into the second relation of equation (11), the following relation for variation of $\phi_2(t)$ in the steady state, is obtained

$$\begin{aligned} &|\phi_{20}|^6 + \frac{8\bar{\omega}^4\sigma}{3\left(\bar{\omega}^2\phi_{1d}^2 - \sigma\right)}|\phi_{20}|^4 \\ &+ \frac{16\bar{\omega}^6\left(\alpha^2\bar{\omega}^4\phi_{1d}^2 + \alpha^2\sigma^2 - 2\alpha^2\bar{\omega}^2\phi_{1d}^2\sigma + \omega_0^2\sigma^2\right)}{9\left(\bar{\omega}^2\phi_{1d}^2 - \sigma\right)^2\beta^2} \\ &\times |\phi_{20}|^2 - \frac{16\phi_{1d}^4\phi_{1o}^2F^2\bar{\omega}^{10}}{9\left(\sigma^2 + \bar{\omega}^4\phi_{1d}^4 - 2\bar{\omega}^2\phi_{1d}^2\sigma\right)\beta^2} = 0 \end{aligned} \tag{12}$$

In this equation ϕ_{20} indicates fixed points of $\phi_2(t)$. On the other hand, ϕ_{20} is a proper approximation of $w(t)$, therefore, for higher values of ϕ_{20}, the NES displacement relative to the beam is more increased and the absorber is more efficient. Assuming $Z = |\phi_{20}|^2$ and substituting it into equation (12) gives

$$\begin{aligned} &\alpha_3 Z^3 + \alpha_2 Z^2 + \alpha_1 Z + \alpha_4 = 0, \\ &\alpha_1 = \frac{16\bar{\omega}^6\left(\alpha^2\bar{\omega}^4\phi_{1d}^2 + \alpha^2\sigma^2 - 2\alpha^2\bar{\omega}^2\phi_{1d}^2\sigma + \omega_0^2\sigma^2\right)}{9\left(\bar{\omega}^2\phi_{1d}^2 - \sigma\right)^2\beta^2}, \\ &\alpha_2 = \frac{8\bar{\omega}^4\sigma}{3\left(\bar{\omega}^2\phi_{1d}^2 - \sigma\right)}, \quad \alpha_3 = 1, \\ &\alpha_4 = -\frac{16\phi_{1d}^4\phi_{1o}^2F^2\bar{\omega}^{10}}{9\left(\sigma^2 + \bar{\omega}^4\phi_{1d}^4 - 2\bar{\omega}^2\phi_{1d}^2\sigma\right)\beta^2} \end{aligned} \tag{13}$$

equation (13) has one or three responses depending on the magnitude of parameters in this equation. In addition, equation (13) reveals that the response of the system is continuous; therefore, a series of bifurcation points including the saddle-node and Hopf bifurcations in the response of the system would occur. In order to determine saddle node bifurcations, derivatives of equation (13) should be equal to zero (Nayfeh and Balachandran, 2004)

$$3\alpha_3 Z^2 + 2\alpha_2 Z + \alpha_1 = 0 \tag{14}$$

Furthermore, equation (14), which shows the necessary condition of the saddle node bifurcation, should be

applied to equation (13). Eliminating z from these two-coupled equations ((13) and (14)), the boundary of existence of the saddle node bifurcation as a function of the system parameters can be obtained.

Furthermore, condition of existence of the Hopf bifurcation can be obtained by introducing the small complex quantities of perturbations, $\delta_1(t)$ and $\delta_2(t)$, around the equilibrium points. Reintroducing the slow-varying modulation as

$$\phi_1(t) = \phi_{10} + \delta_1(t), \quad \phi_2(t) = \phi_{20} + \delta_2(t) \tag{15}$$

Substituting equation (15) into equation (11) and ignoring the nonlinear terms of perturbations, four coupled ordinary differential equations around the equilibrium point are obtained

$$\begin{aligned}
\dot{\delta}_1 = {} & \frac{1}{8\omega_0^3(1+\varepsilon)}\{\varepsilon\{4i\varepsilon\sigma\bar{\omega}^2\delta_2 - 3i\varepsilon\beta\phi_{20}^2\delta_2^* \\
& + 4\alpha\bar{\omega}^3\delta_2 + 6i\beta\phi_{1d}^2\delta_2|\phi_{20}|^2 - 6i\beta\delta_2|\phi_{20}|^2 \\
& + 4i\bar{\omega}^4\delta_2 + 6i\varepsilon\beta\phi_{1d}^2\delta_2|\phi_{20}|^2 - 4i\bar{\omega}^4\delta_1 \\
& + 4i\sigma\bar{\omega}^2\delta_1 - 4\varepsilon\alpha\phi_{1d}^2\bar{\omega}^3\delta_2 - 3i\beta\phi_{20}^2\delta_2^* \\
& - 4\alpha\bar{\omega}^3\phi_{1d}^2\delta_2 + 4\alpha\bar{\omega}^3\varepsilon\delta_2 + 3i\beta\phi_{1d}^2\phi_{20}^2\delta_2^* \\
& + 3i\varepsilon\beta\phi_{1d}^2\phi_{20}^2\delta_2^* - 6i\beta\phi_{1d}^2\phi_{20}^2\delta_2\}\} \\
\dot{\delta}_1^* = {} & \frac{1}{8\bar{\omega}^3(1+\varepsilon)}\{\varepsilon\{4\alpha\bar{\omega}^3\delta_2^* - 4i\varepsilon\sigma\bar{\omega}^2\delta_2^* \\
& + 6i\varepsilon\beta\delta_2^*|\phi_{20}|^2 + 6i\beta\delta_2^*|\phi_{20}|^2 - 4\varepsilon\alpha\phi_{1d}^2\bar{\omega}^3\delta_2^* \\
& - 4\alpha\phi_{1d}^2\bar{\omega}^3\delta_2^* + 4i\bar{\omega}^4\delta_1^* - 6i\varepsilon\beta\delta_2^*|\phi_{20}|^2\phi_{1d}^2 \\
& + 3i\varepsilon\beta\phi_{20}^2\delta_2 - 4i\bar{\omega}^4\delta_2^* - 3i\beta\phi_{1d}^2\phi_{20}^{*2}\delta_2 \\
& - 3i\varepsilon\beta\phi_{1d}^2\phi_{20}^{*2}\delta_2 - 6i\beta\phi_{1d}^2|\phi_{20}|^2\delta_2^* \\
& + 3i\beta\phi_{20}^{*2}\delta_2 - 4i\sigma\bar{\omega}^2\delta_1^*\}\} \\
\dot{\delta}_2 = {} & \frac{1}{8\bar{\omega}^3(1+\varepsilon)}\{-4\alpha\bar{\omega}^3\delta_2 - 4\varepsilon\alpha\phi_{1d}^2\bar{\omega}^3\delta_2 \\
& - 4\varepsilon^2\alpha\phi_{1d}^2\bar{\omega}^3\delta_2 + 3i\varepsilon\beta\phi_{20}^2\delta_2^* - 4\alpha\bar{\omega}^3\varepsilon\delta_2 \\
& + 6i\beta\delta_2|\phi_{20}|^2 - 4i\bar{\omega}^4\delta_2 + 4i\varepsilon^2\beta\phi_{1d}^2\phi_{20}^2\delta_2^* \\
& + 4i\varepsilon\sigma\bar{\omega}^2\delta_1 + 6i\varepsilon^2\beta\phi_{1d}^2\delta_2|\phi_{20}|^2 + 6i\varepsilon\beta\phi_{1d}^2\delta_2|\phi_{20}|^2 \\
& + 4i\bar{\omega}^4\delta_1 + 4i\bar{\omega}^2\varepsilon^2\sigma\delta_2 + 3i\beta\phi_{20}^2\delta_2^* \\
& + 3i\varepsilon\beta\phi_{1d}^2\phi_{20}^2\delta_2^* + 6i\varepsilon\beta\delta_2|\phi_{20}|^2\} \\
\dot{\delta}_2^* = {} & \frac{1}{8\bar{\omega}^3(1+\varepsilon)}\{-4\alpha\bar{\omega}^2\delta_2^* - 4\varepsilon\alpha\phi_{1d}^2\bar{\omega}^3\delta_2^* \\
& - 4\varepsilon^2\alpha\phi_{1d}^2\bar{\omega}^3\delta_2^* - 6i\varepsilon^2\beta\phi_{1d}^2\delta_2^*|\phi_{20}|^2 - 4\alpha\bar{\omega}^3\varepsilon\delta_2^* \\
& - 4i\varepsilon\sigma\bar{\omega}^2\delta_1^* - 3i\varepsilon^2\beta\phi_{1d}^2\delta_2\varphi_{20}^{*2} - 3i\beta\delta_2\phi_{20}^{*2} \\
& - 3i\varepsilon\beta\phi_{1d}^2\delta_2\phi_{20}^{*2} - 4i\varepsilon^2\sigma\delta_2^*\bar{\omega}^2 + 4i\bar{\omega}^4\delta_2^* \\
& - 6i\varepsilon\beta\phi_{1d}^2|\phi_{20}|^2\delta_2^* - 6i\varepsilon\beta|\phi_{20}|^2\delta_2^* \\
& - 6i\beta|\phi_{20}|^2\delta_2^* - 3i\varepsilon\beta|\phi_{20}|^2\delta_2\}
\end{aligned} \tag{16}$$

The stars in equation (16) indicate the complex conjugate of the corresponding parameters. The characteristic polynomial equation of these four coupled equations is

$$\mu^4 + \gamma_1\mu^3 + \gamma_2\mu^2 + \gamma_3\mu + \gamma_4 = 0 \tag{17}$$

The coefficients of equation (17) are presented in Appendix B. The Hopf bifurcation takes place when the characteristic polynomial has a pair of pure complex-conjugate roots as $\mu = \pm j\Omega'$. In fact, Ω' is the characteristic frequency of the periodic orbits and is generated from the bifurcation of the fixed points. Substituting this relation into equation (17) and separating the real and imaginary parts of the equation gives

$$\gamma_3^2 - \gamma_2\gamma_3\gamma_1 + \gamma_4\gamma_1^2 = 0 \tag{18}$$

Equation (18) is the condition of occurrence of the Hopf bifurcation. Simplifying equation (18) and assuming $Z = |\phi_{20}|^2$, it can be written

$$v_1 Z^2 + v_2 Z + v_3 = 0 \tag{19}$$

The coefficients of equation (19) are presented in Appendix C. Furthermore, equation (19), which shows the necessary condition of the Hopf bifurcation, should be applied to equation (13). Eliminating z from these two-coupled equations ((13) and (19)), the boundary of occurrence of the Hopf bifurcation as a function of the system parameters can be specified.

3.2. Analysis of occurrence of strongly modulated responses (SMR)

The fact that the response of the system highly depends on the initial conditions is one of the important points in the analysis of the nonlinear systems. The analysis of the last section are local, hence, they are true only for the initial conditions which are close enough to the stable responses. The existence of SMR was analyzed based on Vakakis et al. (2008). In order to study the strongly modulated responses of the system, equation (11) is used. Determining $\phi_1(t)$ and its derivatives in terms of $\phi_2(t)$ from the second relation of equation (11) and substituting it into the first relation of equation (11), the following second order differential equation is obtained

$$\begin{aligned}
& \frac{d^2\phi_2}{dt^2} + \left\{\frac{-i\varepsilon\sigma}{2\bar{\omega}} + \frac{\varepsilon\alpha\phi_{1d}^2 + \alpha + i\bar{\omega}}{2}\right\}\frac{d\phi_2}{dt} \\
& \quad - \frac{3i\beta}{8\bar{\omega}^3}(\varepsilon\phi_{1d}^2 + 1)\frac{d}{dt}\{\phi_2|\phi_2|^2\} \\
& \quad + \left\{\frac{i\bar{\omega}\varepsilon\alpha\phi_{1d}^2}{4} - \frac{i\varepsilon\sigma\alpha}{4\bar{\omega}} + \frac{\varepsilon\sigma}{4}\right\}\phi_2
\end{aligned}$$

$$+\left\{\frac{3\varepsilon\beta\phi_{1d}^2}{16\bar{\omega}^2}-\frac{3\varepsilon\sigma\beta}{16\bar{\omega}^4}\right\}\phi_2|\phi_2|^2-\frac{i\bar{\omega}F\phi_{1o}\varepsilon\phi_{1d}^2}{4}=0 \quad (20)$$

To solve the above equation, the method of multiple scales is used. For this purpose, the following time scales are introduced

$$\tau_r=\varepsilon^r t,\quad r=0,1,\ldots \quad (21)$$

Thus, the relations between the derivatives of t and the time scales are

$$\begin{aligned}\phi_2&=\phi_2(\tau_0,\tau_1,\ldots),\\ \frac{d}{dt}&=\frac{d}{d\tau_0}+\varepsilon\frac{d}{d\tau_1}+\ldots,\\ \frac{d^2}{dt^2}&=\frac{d^2}{d\tau_0^2}+2\varepsilon\frac{d^2}{d\tau_0 d\tau_1}+\ldots\end{aligned} \quad (22)$$

Substituting equations (22) and (21) into equation (20) and equating the coefficients of the same power of ε, the following relations are achieved

$$\begin{aligned}O(\varepsilon^0):\ &\frac{\partial^2\phi_2}{\partial\tau_0^2}+\left[\frac{i\bar{\omega}+\alpha}{2}\right]\frac{\partial\varphi_2}{\partial\tau_0}-\frac{3i\beta}{8\bar{\omega}^3}\frac{\partial}{\partial\tau_0}\left[\phi_2|\phi_2|^2\right]=0\\ O(\varepsilon^1):\ &2\frac{\partial^2\phi_2}{\partial\tau_0\partial\tau_1}+\left[\frac{i\bar{\omega}+\alpha}{2}\right]\frac{\partial\phi_2}{\partial\tau_1}-\frac{3i\beta}{8\bar{\omega}^3}\frac{\partial}{\partial\tau_1}\left[\phi_2|\phi_2|^2\right]\\ &+\left[\frac{\alpha\phi_{1d}^2}{2}-\frac{i\sigma\bar{\omega}}{2}\right]\frac{\partial\varphi_2}{\partial\tau_0}-\frac{3i\beta\phi_{1d}^2}{8}\frac{\partial}{\partial\tau_0}\left[\phi_2|\phi_2|^2\right]\\ &+\left[\frac{i\bar{\omega}\alpha\phi_{1d}^2}{2}+\frac{\sigma}{4}-\frac{i\sigma\alpha}{4\bar{\omega}}\right]\phi_2+\left[\frac{3\beta\phi_{1d}^2}{16\bar{\omega}^2}-\frac{3\sigma\beta}{16\bar{\omega}^4}\right]\phi_2|\phi_2|^2\\ &-\frac{i\bar{\omega}F\phi_{1o}\phi_{1d}^2}{4}=0\\ O(\varepsilon^2):\ &\ldots\end{aligned} \quad (23)$$

The first expression of equation (23) is related to the fastest time. By integrating this equation, the following equation is obtained

$$\frac{\partial\phi_2}{\partial\tau_0}+\left[\left\{\frac{i\bar{\omega}+\alpha}{2}\right\}\phi_2-\frac{3i\beta}{8\bar{\omega}^3}\phi_2|\phi_2|^2\right]=E(\tau_1,\tau_2,\ldots) \quad (24)$$

In this study, responses that are limited to the time-scales τ_0 and τ_1 are considered. When $\tau_0\to\infty$, parameters in τ_0 order stay invariant and ϕ_2 reaches an asymptotic equilibrium where $\phi_2=\phi_2(\tau_1)$ ($\tau_0\to\infty:\frac{\partial\phi_2}{\partial\tau_0}=0$). Accordingly, the equation (24) can be written as follow

$$\left[\left\{\frac{i\bar{\omega}+\alpha}{2}\right\}\phi_2(\tau_1)-\frac{3i\beta}{8\bar{\omega}^3}\phi_2(\tau_1)\left|\phi_2(\tau_1)\right|^2\right]=E(\tau_1) \quad (25)$$

Expressing the complex quantities of equation (25) in the polar form ($\phi_2(\tau_1)=N(\tau_1)e^{i\gamma(\tau_1)}$), and rewriting it, gives

$$\begin{aligned}&\frac{\alpha N(\tau_1)}{2}e^{i\gamma(\tau_1)}+\left[\frac{\bar{\omega}N(\tau_1)}{2}-\frac{3\beta N^3(\tau_1)}{8\bar{\omega}^3}\right]ie^{i\gamma(\tau_1)}\\ &=\left|E(\tau_1)\right|e^{i\arg(E(\tau_1))}\end{aligned} \quad (26)$$

Using the above equation and assuming $Z(\tau_1)=N^2(\tau_1)$, the following relation is obtained for the magnitude of the equation terms

$$\left[\frac{\alpha}{2}\right]^2Z(\tau_1)+\left[\frac{\bar{\omega}}{2}-\frac{3\beta Z(\tau_1)}{8\bar{\omega}^3}\right]^2Z(\tau_1)=\left|E(\tau_1)\right|^2 \quad (27)$$

The relation between angles of the parameters in equation (26) is derived as

$$\gamma(\tau_1)=\arg(\left|E(\tau_1)\right|)+\tan^{-1}\left(\frac{3\beta Z(\tau_1)-4\bar{\omega}^4}{4\alpha\bar{\omega}^3}\right) \quad (28)$$

The number of solutions of equation (27) depends on the magnitude of α, β, $\bar{\omega}$ and $\left|E(\tau_1)\right|$. If equation (27) has minimum and maximum points, this equation depending on the magnitude of $\left|E(\tau_1)\right|$ has one or three solutions. In this case, due to change of $\left|E(\tau_1)\right|$, the system can produce the saddle-node bifurcations, and therefore, the stable and unstable branches occur. However, if equation (27) has no extremum points, this equation has one solution. It is important to note that if the differentiation of homogenous part of equation (27) has real solutions, the extrema can be obtained as follows

$$\begin{aligned}&\frac{d}{dZ}\left\{\left[\frac{\alpha}{2}\right]^2Z(\tau_1)+\left[\frac{\bar{\omega}}{2}-\frac{3\beta Z(\tau_1)}{8\bar{\omega}^3}\right]^2Z(\tau_1)\right\}\\ &=0\Rightarrow Z_{1,2}=\frac{4\bar{\omega}^3}{3\beta}\left[\frac{2}{3}\bar{\omega}\mp\frac{1}{3}\sqrt{\bar{\omega}^2-3\alpha^2}\right]\end{aligned} \quad (29)$$

equation (29) indicates that for $\alpha<\bar{\omega}/\sqrt{3}$ (small damping), the system has a pair of solutions and the saddle-node bifurcations occur. Also, for $\alpha>\bar{\omega}/\sqrt{3}$, the system has one solution and the saddle-node bifurcation does not occur at all (Gendelman, 2004). Figure 2 shows the slow invariant manifold diagram of the system with parameters: $\alpha=0.5$, $\beta=1$ and $\bar{\omega}=1.24$. This concept was used based on Fenichel (2006) and Savadkoohi et al. (2012). The jump phenomenon, which is the fast part of the slow-varying response of the system, the stable and unstable responses and the saddle-node bifurcations, is shown in Figure 2.

Since, there are two stable regions in the system response, the jump phenomenon may occur between

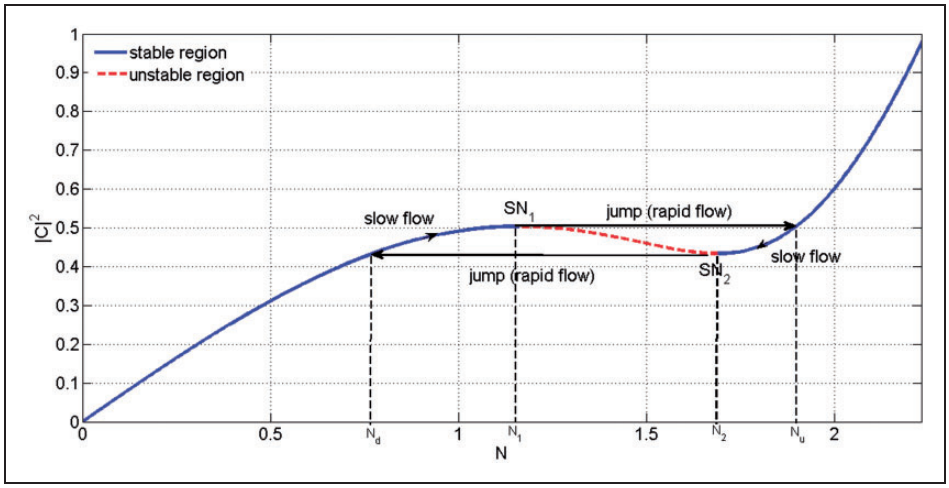

Figure 2. The slow invariant manifold diagram of the system with $\alpha = 0.5$, $\beta = 1$ and $\bar{\omega} = 1.24$; the jump phenomena and the saddle-node bifurcations.

these regions. In order to investigate the occurrence of jump phenomenon, the system response near the slow invariant manifold in the time order τ_1 when $\tau_0 \to \infty$ should be studied. When $\tau_0 \to \infty$, parameters in τ_0 order stay invariant. However, the time scale τ_1 is slower than τ_0, consequently, these parameters varies in the order of τ_1. Assuming $\Phi(\tau_1) = \lim_{\tau_0 \to \infty} \phi_2(\tau_0, \tau_1)$ and considering the above notes, the relation of order ε in equation (23) becomes as the following

$$\left[\frac{i\bar{\omega}+\alpha}{2}\right]\frac{\partial\Phi}{\partial\tau_1} - \frac{3i\beta}{8\bar{\omega}^3}\frac{\partial}{\partial\tau_1}[\Phi|\Phi|^2] + \left[\frac{i\bar{\omega}\alpha\phi_{1d}^2}{2} + \frac{\sigma}{4} - \frac{i\sigma\alpha}{4\bar{\omega}}\right]\Phi + \left[\frac{3\beta\phi_{1d}^2}{16\bar{\omega}^2} - \frac{3\sigma\beta}{16\bar{\omega}^4}\right]\Phi|\Phi|^2 - \frac{i\bar{\omega}F\phi_{1o}\phi_{1d}^2}{4} = 0 \quad (30)$$

Rewriting the above equation gives

$$\left[\frac{i\bar{\omega}+\alpha}{2} - \frac{3i\beta}{4\bar{\omega}^3}|\Phi|^2\right]\frac{\partial\Phi}{\partial\tau_1} - \frac{3i\beta\Phi}{8\bar{\omega}^3}\frac{\partial\Phi^*}{\partial\tau_1} = G,$$
$$G = \left[\frac{i\sigma\alpha}{4\bar{\omega}} - \frac{i\bar{\omega}\alpha\phi_{1d}^2}{2} - \frac{\sigma}{4}\right]\Phi + \frac{i\bar{\omega}F\phi_{1o}\phi_{1d}^2}{4} + \left[\frac{3\sigma\beta}{16\bar{\omega}^4} - \frac{3\beta\phi_{1d}^2}{16\bar{\omega}^2}\right]\Phi|\Phi|^2 \quad (31)$$

In order to obtain the expression of $\frac{\partial\Phi}{\partial\tau_1}$ which demonstrates the variations of the slow dynamics of the system around the slow invariant manifold, equation (31) and its conjugate are written in a matrix form. Solving these coupled equations, the following result can be obtained

$$\frac{\partial\Phi}{\partial\tau_1} = \frac{8\bar{\omega}^3[[4\alpha\bar{\omega}^3 - 4i\bar{\omega}^4 + 6i\beta|\Phi|^2]G + 3i\beta\Phi^2G^*]}{16\alpha^2\bar{\omega}^6 + 16\bar{\omega}^8 - 48\bar{\omega}^4\beta|\Phi|^2 + 27\beta^2|\Phi|^4} \quad (32)$$

Assuming $\Phi = N(\tau_1)e^{i\gamma(\tau_1)}$ and substituting it into equation (32), the following relation is obtained

$$\left[\frac{i\bar{\omega}+\alpha}{2} - \frac{3i\beta}{4\omega_0^3}N(\tau_1)^2\right] \times \left[\left(\frac{\partial N(\tau_1)}{\partial\tau_1} + iN(\tau_1)\frac{\partial\gamma(\tau_1)}{\partial\tau_1}\right)e^{i\gamma(\tau_1)}\right] - \frac{3i\beta N(\tau_1)e^{i\gamma(\tau_1)}}{8\omega_0^3}\left[\left(\frac{\partial N(\tau_1)}{\partial\tau_1} - iN(\tau_1)\frac{\partial\gamma(\tau_1)}{\partial\tau_1}\right)e^{-i\gamma(\tau_1)}\right]$$
$$= \left[\frac{i\sigma\alpha}{4\bar{\omega}} - \frac{i\bar{\omega}\alpha\phi_{1d}^2}{2} - \frac{\sigma}{4}\right]N(\tau_1)e^{i\gamma(\tau_1)} + \frac{i\bar{\omega}F\phi_{1o}\phi_{1d}^2}{4} + \left[\frac{3\sigma\beta}{16\bar{\omega}^4} - \frac{3\beta\phi_{1d}^2}{16\bar{\omega}^2}\right]N(\tau_1)^3e^{i\gamma(\tau_1)} \quad (33)$$

Separating real and imaginary parts of the above equations, gives two ordinary differential equations and solving them for $\frac{\partial N(\tau_1)}{\partial\tau_1}$ and $\frac{\partial\gamma(\tau_1)}{\partial\tau_1}$ gives

$$\frac{\partial N(\tau_1)}{\partial\tau_1} = \frac{\left\{\begin{array}{c} 2\bar{\omega}^2\phi_{1d}^4[4\bar{\omega}^3\alpha F\sin(\gamma(\tau_1)) + 4\bar{\omega}^4F\phi_{1o}\cos(\gamma(\tau_1)) \\ -3N(\tau_1)^2\cos(\gamma(\tau_1))F\phi_{1o}\beta - 4N(\tau_1)\bar{\omega}^4\alpha] \end{array}\right\}}{[16\bar{\omega}^8 + 16\alpha^2\bar{\omega}^6 + 27\beta^2N(\tau_1)^4 - 48\bar{\omega}^4N(\tau_1)^2\beta]}$$

$$\frac{\partial\gamma(\tau_1)}{\partial\tau_1} = [16\bar{\omega}^8F\phi_{1o}\phi_{1d}^2\cos(\gamma(\tau_1))\alpha - 16\bar{\omega}^9F\phi_{1o}\phi_{1d}^2\sin(\gamma(\tau_1)) + 16N(\tau_1)\bar{\omega}^8\sigma + 27\beta^2\sigma N(\tau_1)^5 - 27\beta^2N(\tau_1)^5\phi_{1d}^2\bar{\omega}^2 - 48\bar{\omega}^4\sigma\beta N(\tau_1)^3 + 16\sigma\alpha^2N(\tau_1)\bar{\omega}^6 - 16\bar{\omega}^8\alpha^2N(\tau_1)\phi_{1d}^2 + 12\beta N(\tau_1)^3\phi_{1d}^2\bar{\omega}^6 + 36\bar{\omega}^5F\phi_{1o}\phi_{1d}^2\sin(\gamma(\tau_1))\beta N(\tau_1)^2] / [2\bar{\omega}N(\tau_1)[16\bar{\omega}^8 + 16\alpha^2\bar{\omega}^6 + 27\beta^2N(\tau_1)^4 - 48\bar{\omega}^4N(\tau_1)^2\beta]] \quad (34)$$

The possibility of occurrence of the SMR can be investigated using phase plane plots of equation (34). This coupled equations give wealthy information about dynamics of the system at slow time scale. Equilibrium points are those which give numerators = 0 but denominator ≠ 0. Fold singularities which can provide SMR are those which satisfy numerators = 0 and denominator = 0. In addition, denominator = 0 provides fold lines of the system (Lamarque et al., 2011; Gendelman, 2008). It is obvious that, the amplitude of the system with damping and without external excitation, approaches to zero. However, the necessary condition for occurrence of the SMR is a jump phenomenon from low to high amplitudes of the stable slow invariant manifold that has been demonstrated in Figure 2. The jump phenomenon occurs when the saddle-node bifurcation takes place in the $N(\tau_1) - \gamma(\tau_1)$ phase space at the low critical amplitudes (i.e. as shown in Figure 8), which is equivalent to points SN_1 in Figure 2. It means that the direction of the dynamic flows in the lower branch is upward which is in contrast to the standard case (the behavior of the system with damping and without external excitation). In order to evaluate the amplitude of the external excitation by which the saddle-node bifurcation occurs, the numerator of equation (32) should be equal to zero (Manevitch, 2001; Lee et al., 2007)

$$\begin{aligned}&\frac{1}{128\omega_0^7}\big[16i\alpha\bar{\omega}^8F\phi_{1o}\phi_{1d}^2+12i\bar{\omega}^6\beta\Phi|\Phi|^2\phi_{1d}^2\\&-48I\bar{\omega}^4\sigma\beta\Phi|\Phi|^2-16\bar{\omega}^9\alpha\Phi\phi_{1d}^2+16i\alpha^2\bar{\omega}^6\sigma\Phi\\&+16\bar{\omega}^9F\phi_{1o}\phi_{1d}^2-16i\alpha^2\omega_0^8\Phi\phi_{1d}^2-27i\beta^2|\Phi|^4\\&\times\Phi\phi_{1d}^2\bar{\omega}^2+16i\bar{\omega}^8\sigma\Phi-27\beta|\Phi|^2F\phi_{1o}\phi_{1d}^2\bar{\omega}^5\\&+27i\beta^2|\Phi|^4\sigma\Phi+12\beta\Phi^2F\phi_{1o}\phi_{1d}^2\bar{\omega}^5\big]=0\end{aligned}\tag{35}$$

Assuming $\Phi = N(\tau_1)e^{i\gamma(\tau_1)}$ and substituting it into equation (35) and separating the real and imaginary parts of the equation, gives

$$\begin{aligned}&\frac{1}{128\bar{\omega}^7}\big[16\sin(\gamma(\tau))\alpha\bar{\omega}^8F\phi_{1o}\phi_{1d}^2\\&-16\bar{\omega}^9\alpha N(\tau)\Phi\phi_{1d}^2+16\cos(\gamma(\tau))\bar{\omega}^9F\phi_{1o}\phi_{1d}^2\\&-12\cos(\gamma(\tau))\beta N(\tau)^2F\phi_{1o}\phi_{1d}^2\bar{\omega}^5\big]=0\\&\frac{1}{128\bar{\omega}^7}\big[16\cos(\gamma(\tau))\alpha\bar{\omega}^8F\phi_{1o}\phi_{1d}^2+12\bar{\omega}^6\beta N(\tau)^3\phi_{1d}^2\\&-48\bar{\omega}^4\sigma\beta N(\tau)^3+16\alpha^2\bar{\omega}^6\sigma N(\tau)\\&-16\sin(\gamma(\tau))F\bar{\omega}^9\phi_{1o}\phi_{1d}^2-16\alpha^2\bar{\omega}^8N(\tau)\phi_{1d}^2\\&-27\beta^2N(\tau)^5\phi_{1d}^2\bar{\omega}^2+16\bar{\omega}^8N(\tau)\\&+36\sin(\gamma(\tau))\beta N(\tau)^2F\phi_{1o}\phi_{1d}^2\bar{\omega}^5\\&+27\beta^2N(\tau)^5\sigma\big]=0\end{aligned}\tag{36}$$

By solving the above equation for $\cos(\gamma(\tau))$ and $\sin(\gamma(\tau))$ (Lamarque et al., 2011), gives

$$\begin{aligned}\cos(\gamma(\tau))&=\frac{(\phi_{1d}^2\bar{\omega}^2-\sigma)N(\tau)\alpha}{\phi_{1d}^2\bar{\omega}^2F\phi_{1o}},\\\sin(\gamma(\tau))&=\frac{N(\tau)\begin{pmatrix}4\bar{\omega}^4\sigma-3N^2(\tau)\beta\sigma\\+3N^2(\tau)\beta\phi_{1d}^2\bar{\omega}^2\end{pmatrix}}{4\phi_{1d}^2\bar{\omega}^5F\phi_{1o}}\end{aligned}\tag{37}$$

Letting $\sigma = 0$ in equation (37) gives

$$\cos(\gamma(\tau))=\frac{N(\tau)\alpha}{F\phi_{1o}},\quad \sin(\gamma(\tau))=\frac{3N^3(\tau)\beta}{4\bar{\omega}^3F\phi_{1o}}\tag{38}$$

Finally, employing mathematical manipulations, the angle of occurrence of the saddle node bifurcation ($\gamma_{1,2}$) is obtained

$$\begin{aligned}\gamma_{1,2}=&\sin^{-1}\left(\frac{(\alpha/\phi_{1o})}{\sqrt{(\frac{3N(\tau)^2\beta}{4\phi_{1o}\bar{\omega}^3}-1)^2+(\alpha/\phi_{1o})^2}}\right)\\&\mp\cos^{-1}\left(\frac{(-N(\tau)\alpha/F\phi_{1o})}{\sqrt{(\frac{3N(\tau)^2\beta}{4\phi_{1o}\bar{\omega}^3}-1)^2+(\alpha/\phi_{1o})^2}}\right)\end{aligned}\tag{39}$$

Substituting the magnitude of the critical amplitudes N_1 and N_2 from equation (29) into equation (39), gives the angles for which the saddle-node bifurcations occur in the low and high amplitudes, respectively. Using equation (39) and considering absolute value of the argument of $\cos^{-1}$ equal to one, the critical amplitude of the external excitation for occurrence of the saddle-node bifurcations is obtained as

$$F_{critical[i]}=\frac{(N_i\alpha/\phi_{1o})}{\sqrt{\left(\frac{3N_i^2\beta}{4\phi_{1o}\bar{\omega}^3}-1\right)^2+(\alpha/\phi_{1o})^2}}\tag{40}$$

When the external excitation is greater than the amplitude of external excitation related to the first critical amplitude $F_{critical[1]}$, the saddle-node bifurcation occurs in the lower critical amplitude (i.e. as shown in Figure 8). Also, when the external excitation is greater than the amplitude of the excitation related to the second critical amplitude $F_{critical[2]}$, the saddle-node bifurcation occurs in the upper critical amplitude (i.e. as shown in Figure 13). Accordingly, for occurrence of the SMR, the magnitude of the external excitation should be greater than the first critical amplitude ($F > F_{critical[1]}$).

To ensure the occurrence of SMR behavior in the system, a map is assumed, which shows that whether dynamic flow that starts from a point with lower critical amplitude (N_1) and angle between γ_1 and γ_2, after passing through two fast parts of the slow-varying responses (jumps) and two slow parts of the slow-varying response, finally returns to this region or not (these four parts of motion can be seen in the closed loop in the Figures 2 and 10) (Vakakis et al., 2008). This is achieved by examining the dynamic flow angle ($\gamma(\tau_1)$) over time. If the dynamic flow returns to the primary region, surely the SMR has been occurred in the system (e.g. as shown in Figures 9 and 10). In other words, it is the sufficient condition for existence of the SMR behavior. These figures nominate a sustained jumping map. Since, occurrence of the jump phenomenon is very fast, it can be assumed that the total energy of the system ($|C(\tau_1)|$) in equation (27) is constant. Accordingly, as it can be seen in Figure 2, when system jumps from a point with amplitude N_1 to a point with amplitude N_u, by some mathematical manipulations, the amplitude of jump end point (N_u) is obtained as

$$N_u = \sqrt{\frac{8\bar{\omega}^3}{9\beta}\left[\bar{\omega} + \sqrt{\bar{\omega}^2 - 3\alpha^2}\right]} \tag{41}$$

The magnitude of amplitude N_d is obtained, similarly, by letting the energy of the point with this amplitude and the point with amplitude N_2 be equal to each other

$$N_d = \sqrt{\frac{8\bar{\omega}^3}{9\beta}\left[\bar{\omega} - \sqrt{\bar{\omega}^2 - 3\alpha^2}\right]} \tag{42}$$

In order to determine the change of angle in each jump, equation (25) is used. In this relation $C(\tau_1)$ is a constant. Substituting $\varphi_2(\tau_1) = N(\tau_1)e^{i\gamma(\tau_1)}$ into equation (25) and some mathematical manipulations, one has

$$\gamma_u = \gamma_1 + \tan^{-1}\left(\frac{72\sqrt{\bar{\omega}^2 - 3\alpha^2}\alpha}{393\alpha^2 + 41\bar{\omega}^2 + 104\bar{\omega}\sqrt{\bar{\omega}^2 - 3\alpha^2}}\right) \tag{43}$$

Similarly, the change of angle between two points with amplitudes N_2 and N_d is obtained

$$\gamma_d = \gamma_2 - \tan^{-1}\left(\frac{72\alpha\sqrt{\bar{\omega}^2 - 3\alpha^2}}{393\alpha^2 + 41\bar{\omega}^2 - 104\bar{\omega}\sqrt{\bar{\omega}^2 - 3\alpha^2}}\right) \tag{44}$$

4. Numerical solution

The coupled equations of motion of the rotating beam and NES (equation (5)) are transformed to the state space. These first-order outcome equations are numerically solved using the Rung Kutta method.

5. Numerical example

In this section, numerical examples are presented. For this purpose, the following parameters are used: $r_i = 0.5\,\text{m}$, $r_o = 1.5\,\text{m}$, $l = 1\,\text{m}$, $A = 25\,\text{cm}^2$ and, $\rho = 2500\,\text{kg/m}^3$. By assuming that the intake fan in turbine has three blades, the frequency of the external force $\bar{\omega}$ is three times of the angular velocity of the rotating beam, $\bar{\Omega}$. The resonance occurs when the first natural frequency of the rotating beam ($\omega_1 = \sqrt{k'_{11}/m'_{11}}$) is equal to the angular frequency of the external force $\bar{\omega}$. According to the aforementioned values of parameters, this resonance occurs at $\bar{\omega} = 1.24$. It is worth mentioning that for the above-mentioned parameters, the first, second and third natural frequencies are 3.72, 22.37 and 62.05, respectively, and the excitation frequency is 1.24. Therefore, the coupled system of the beam and NES can be considered as a two degrees of freedom system, which includes the first (and the most important) mode of the rotating beam and the NES. In order to obtain the optimal parameters of the NES, existence of the saddle-node bifurcation, Hopf bifurcation, and the amplitude of the external force for occurrence of a strongly modulated response in the parameter space of α, F and d, which are the non-dimensional damping of the NES, non-dimensional amplitude of the external force and non-dimensional distance of the NES position from the root of the rotating beam, respectively, are studied.

Figure 3 shows existence of the saddle-node bifurcation in the parameter space of α, F and d, for $\sigma = 1$. It can be seen that for $0 < d < 0.52$, the saddle-node bifurcation would occur. Therefore, for $\sigma = 1$, if the NES position is at the rotating beam tip, the saddle-node bifurcation does not occur. Moreover, by increasing d, the amplitudes of the external force in which the saddle-node bifurcation happens, are decreased. Also, if the NES position is at the rotating beam root, in a wider range of the NES damping, the saddle-node bifurcation occurs. It is shown that the occurrence of saddle-node bifurcation is dependent on the detuning parameter (σ). For example, for $\sigma = -3$, the saddle-node bifurcation occurs for the entire length of the rotating beam ($0 < d < 1$).

Figure 4 depicts the occurrence of the Hopf bifurcation in the parameter space of α, F and d, for $\sigma = 1$. It can be seen that the Hopf bifurcation takes place for the entire length of the rotating beam ($0 < d < 1$). In addition, in this case, similar to the saddle-node

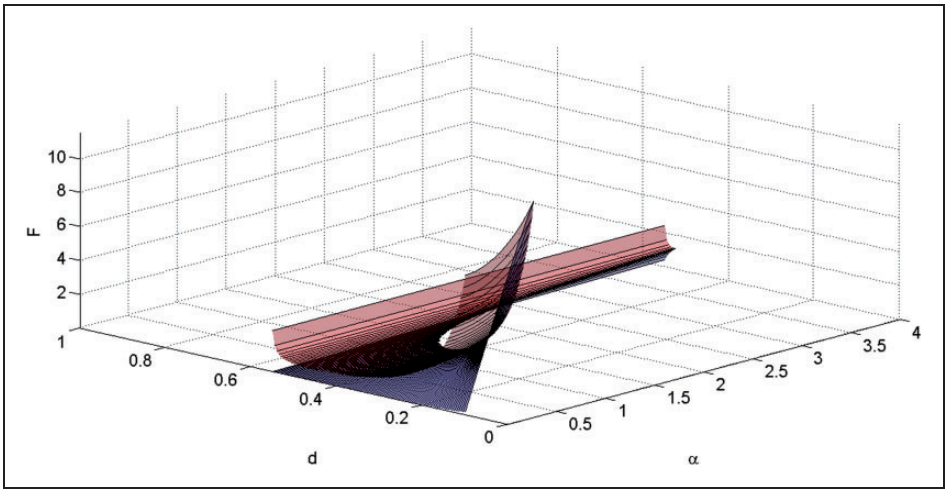

Figure 3. The existence of saddle-node bifurcation in the parameter space of α, F and d for $\sigma = 1$.

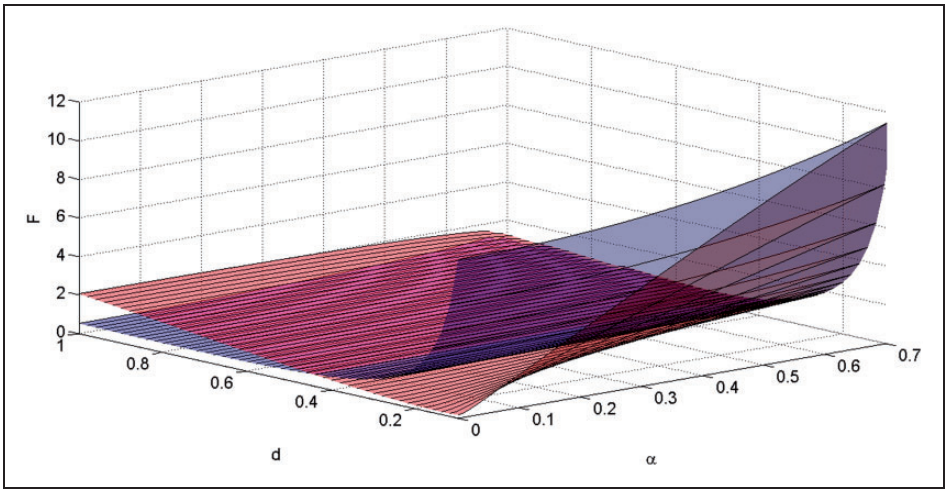

Figure 4. The existence of Hopf bifurcation in the parameter space of α, F and d for $\sigma = 1$.

bifurcation, by increasing d, the amplitudes of the external force in which the Hopf bifurcation happens, are decreased. It is shown that unlike the saddle-node bifurcation, dependency of the existence of the Hopf bifurcation to the detuning parameter (σ) is small.

In Figure 5, the critical amplitude of the external force for occurrence of the SMR in the parameter space is plotted. Unlike the conditions of occurrence of Hopf and saddle bifurcations, the amplitudes of the external force for existence of the SMR behavior are increased by increasing the distance of the absorber position from the base of the rotating beam. As it can be seen, by changing the absorber position, the range of damping in which the SMR occurs, would be invariant. This range would be $0 < \alpha < \bar{\omega}/\sqrt{3}$ and can be obtained from equation (29).

The above results demonstrate that the dynamic behavior of the coupled system of NES and rotating beam is strongly dependent on the position of the NES on the rotating beam (d). Therefore, in order to investigate optimal parameters of the NES, four sections of the rotating beam for connecting the NES to a rotating beam are examined. These sections are selected as $d = 0.3$, $d = 0.5$, $d = 0.86$ and $d = 0.99$. For this purpose, firstly the existence of the Hopf and saddle-node bifurcations and the amplitudes of the external force for occurrence of the SMR in the F-α space are investigated in these sections (Gendelman et al., 2008). Then, for the parameters at which aforementioned bifurcations occur, the amplitude versus detuning parameter (frequency response curve) is illustrated, and the range of the occurrence of the SMR in the detuning parameter region is considered (Vakakis et al., 2008).

The first attachment position of the NES to the rotating beam, at which the dynamic behavior of the

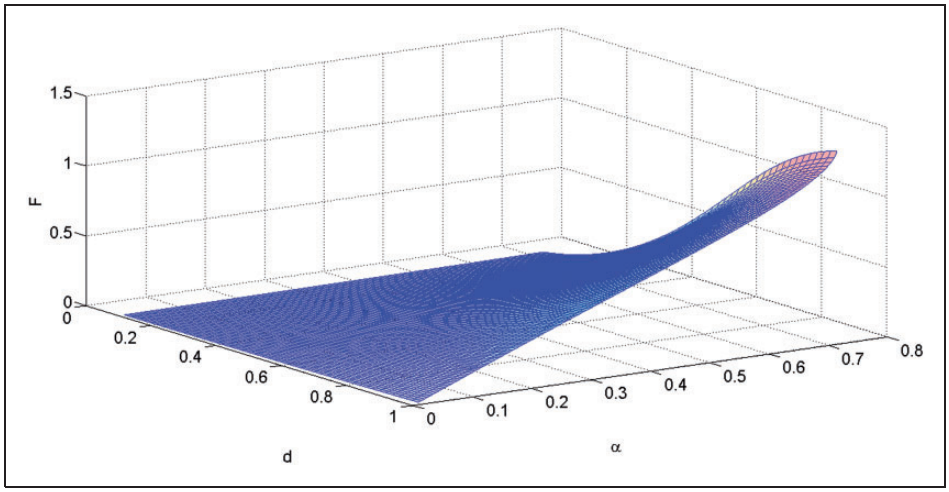

Figure 5. The amplitudes of the external force for occurrence of the SMR in the parameter space of α, F and d.

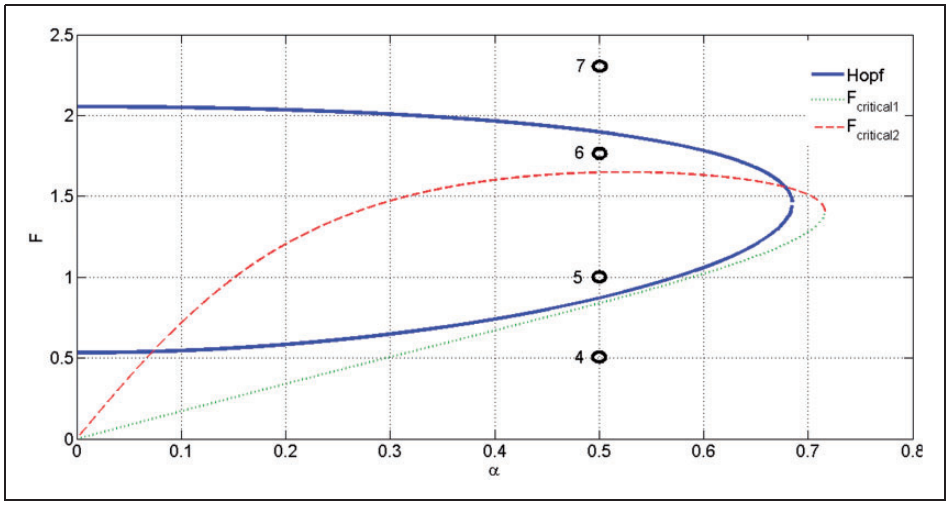

Figure 6. The existence of the Hopf and saddle bifurcations and the amplitudes of the external force for occurrence of the SMR in the $F-\alpha$ space for $\sigma = 1$ and $d = 0.99$.

system is investigated, is at the end of the rotating beam. In this case, spatial parameters of the system are $d = 0.99$, $\phi_{1o} = 1.013$, $\phi_{1d} = 1.972$ for $\sigma = 1$. Figure 6 represents the Hopf and saddle-node bifurcations and the amplitudes of the external force for occurrence of the SMR in the F-α space for this section. As it can be seen, the saddle-node bifurcation does not occur for $\sigma = 1$ at this section. The coupled rotating beam-NES system has a different dynamical behavior, depending on the parameters of the system located at each zone of the F-α space. Therefore, the dynamical behavior of the system in four points of the F-α space are investigated accurately. The numbers of these points in Figure 6 are selected 4, 5, 6 and 7. The phase plane of the slow motion and the sustained jumping map of the system, for the parameters relevant to these points are investigated.

In Figure 7, the phase plane of the slow motion for $d = 0.99$, $\sigma = 1$, $F = 0.5$ and $\alpha = 0.5$ is illustrated. These parameters are relevant to point 4 in Figure 6. It is shown that all trajectories in this figure approach to a node. Since, this figure relates to the slow motion dynamic, the node in this figure demonstrates a periodic motion of the system in the real time (according to equation (10)). The amplitude of the external force corresponding to point 4 in Figure 6 is smaller than the amplitude of the external force for the occurrence of the SMR. Therefore, the system has periodic behavior and the SMR will not occur. It is shown that, the numerical results have a good consistency with the analytical ones

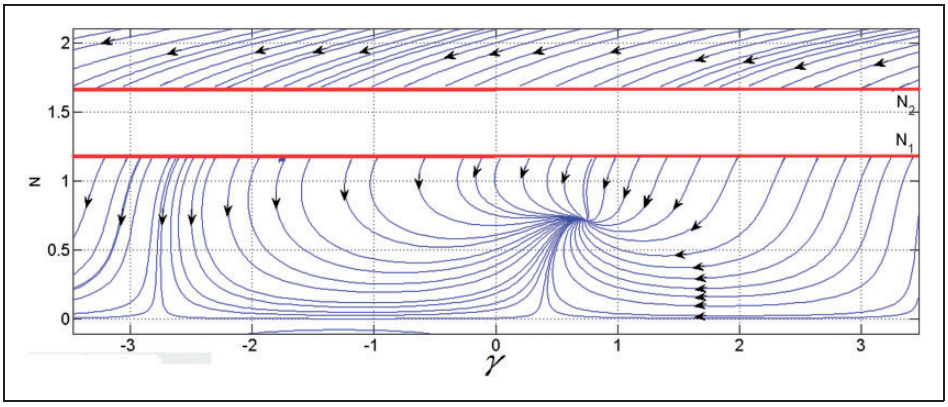

Figure 7. The phase plane of the slow motion of the system for $d = 0.99$, $\sigma = 1$, $F = 0.5$ and $\alpha = 0.5$ (point 4 in Figure 6).

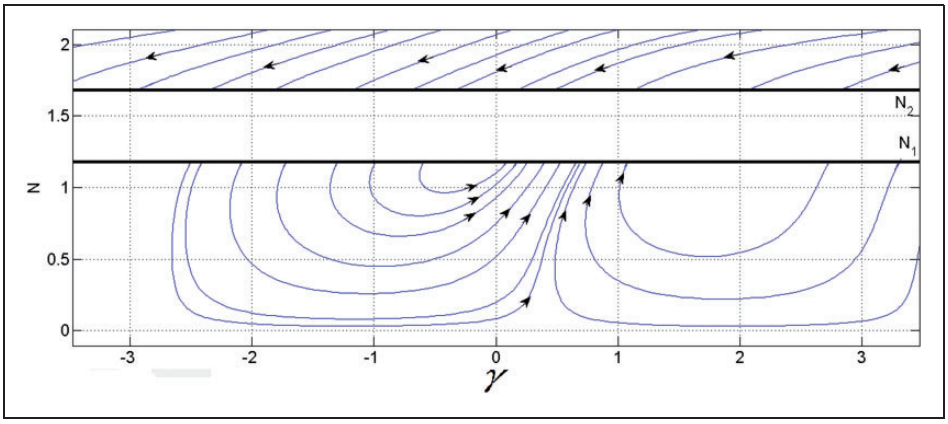

Figure 8. The phase plane of slow motion of the system for $d = 0.99$, $\sigma = 1$, $F = 1$ and $\alpha = 0.5$ (point 5 in Figure 6).

and the system is attracted to a periodic motion for any arbitrary initial condition and the SMR and WMR for all values of (σ) would not occur.

The phase portrait of the slow motion for $d = 0.99$, $\sigma = 1$, $F = 1$ and $\alpha = 0.5$ is shown in Figure 8. These parameters are related to point 5 in Figure 6. It can be seen in Figure 8, since the bifurcations exist in the lower critical amplitude (N_1), a jump from the lower amplitude to an upper amplitude takes place. This phenomenon is a probable reason of the SMR. To ensure the occurrence of SMR, the sustained jumping map is plotted in Figure 9. In this figure, the end angle of the dynamic flow is obtained after thousand oscillations, (each oscillation includes two jumps and two slow parts of the slow-varying response). As it can be seen, all trajectory angles approach to a unit angle ($\gamma = 0.2$ radian). This result shows that the SMR occurs in the system. The trajectory of the system in the slow motion is demonstrated in Figure 10. All trajectories approach a closed loop, which is a demonstrator of the SMR in this space.

In Figure 11, the frequency response curves of the system are plotted for aforementioned parameters. As it can be seen, the saddle-node and hopf bifurcations occur in this case. Also, for some values of σ, there are three types of responses. It should be noted that for $-4.4 < \sigma < 12.1$ and $-4.47 < \sigma < 2.64$, the SMR and the WMR (Hopf bifurcation) occur, respectively. For $6 < \sigma < 11$, the high amplitude periodic motion exists. It is seen that for $\sigma = 8$, three different solutions take place as the high amplitude periodic motion, low amplitude periodic motion and SMR. The numerical results demonstrate that only the low amplitude periodic motion occur for $\sigma = 8$. Also, for $\sigma = -2$, based on this analytical results, two different responses exist as the WMR and the SMR. But the numerical results illustrate that only the SMR exists for $\sigma = -2$. In this case, due to the existence of the SMR, the dynamic behavior of the system does not approach to the WMR. The temporal response of the system with an arbitrary initial condition for the above-mentioned parameters is shown in Figure 12 to demonstrate that

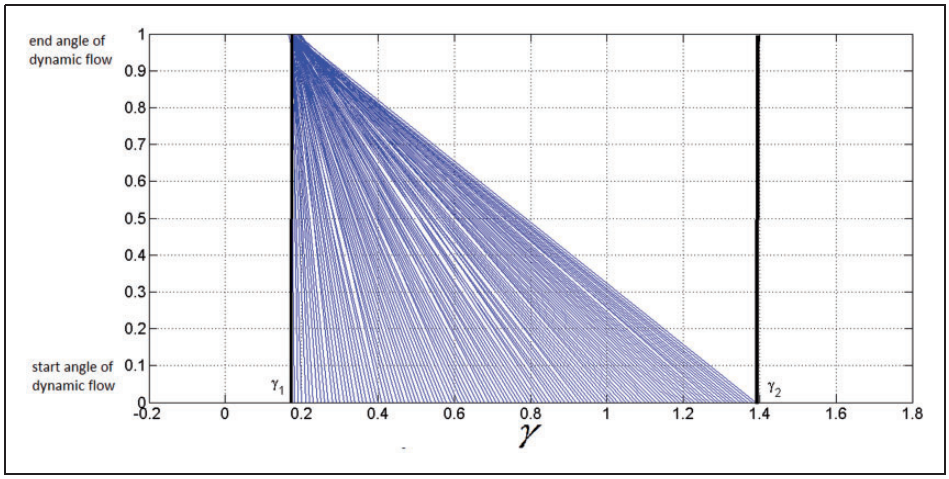

Figure 9. The sustained jumping map for $d = 0.99$, $\sigma = 1$, $F = 1$ and $\alpha = 0.5$ (point 5 in Figure 6).

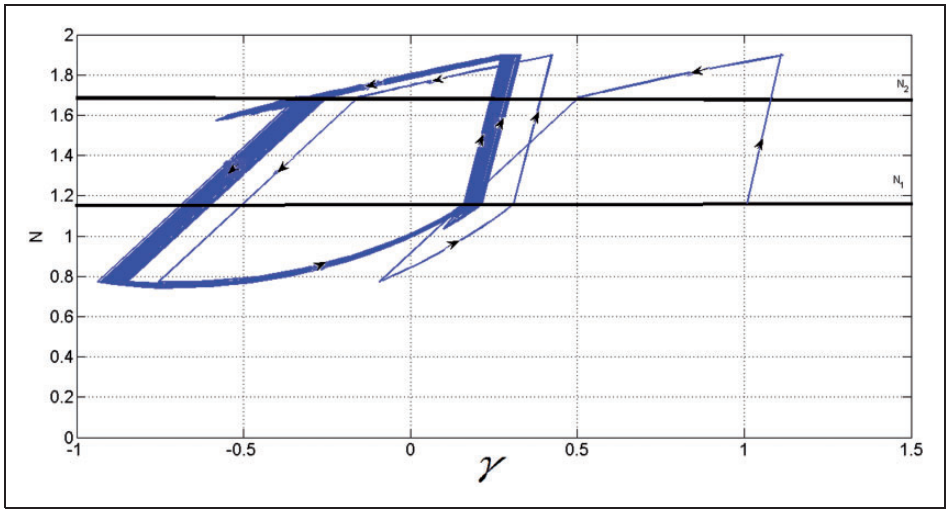

Figure 10. The trajectory of the slow motion of the system in the phase plane for $d = 0.99$, $\sigma = 1$, $F = 1$ and $\alpha = 0.5$ (point 5 in Figure 6.

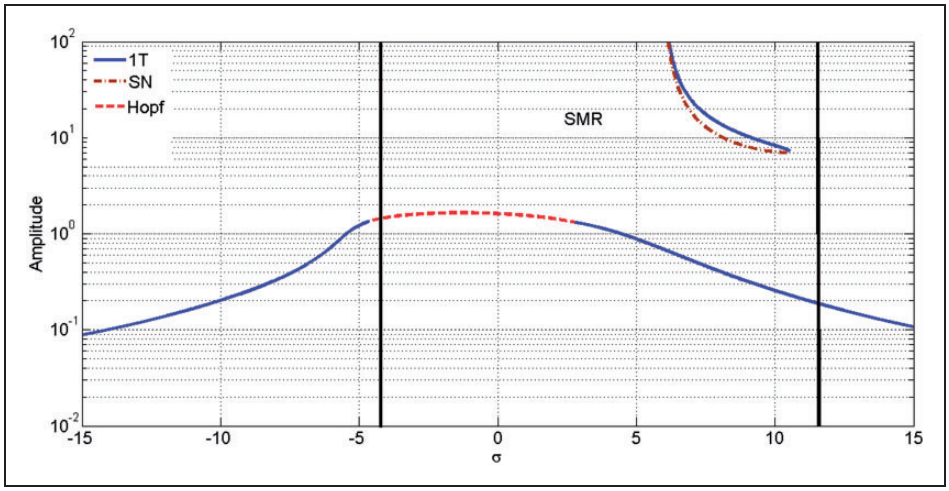

Figure 11. The Frequency response curves of the system for $d = 0.99$, $\alpha = 0.5$ and $F = 1$ (point 5 in Figure 6).

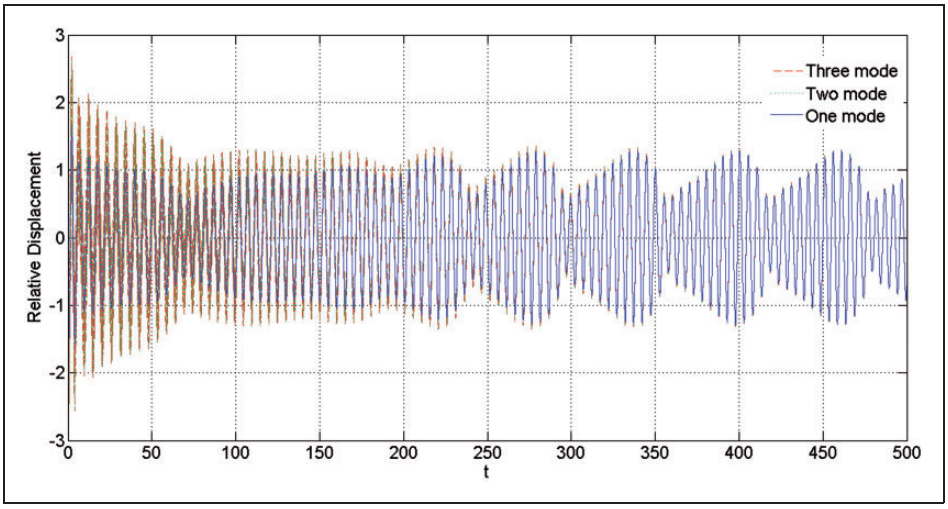

Figure 12. Time response of the system (occurrence of the SMR) for $d = 0.99$, $\alpha = 0.5$ and $F = 1$ (point 5 in Figure 6) and $\sigma = -2$.

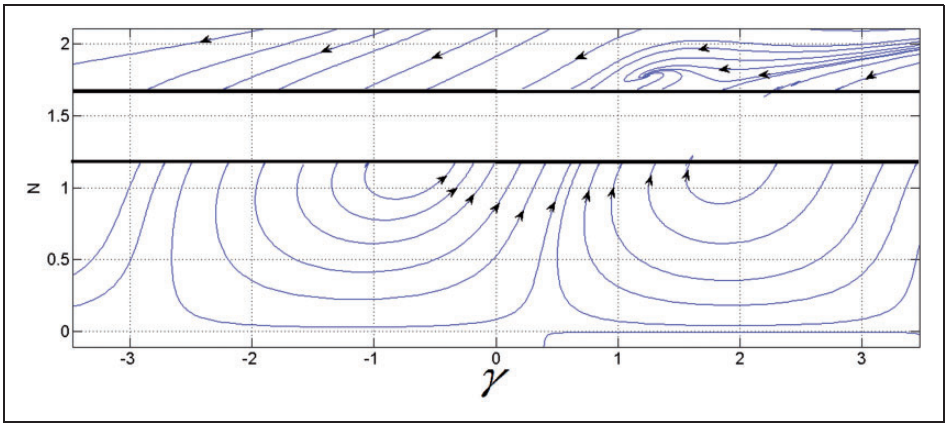

Figure 13. The Phase plane of slow motion of the system for $d = 0.99$, $\sigma = 1$, $F = 2$ and $\alpha = 0.5$ (point 7 in Figure 6).

the system has SMR in the time domain. Additionally, the temporal response of the system with two and three first Galerkin modes are depicted in this figure. It is obvious that the steady state response of the system with the first one, two or three Galerkin modes are equal to each other. Indeed, this figure proves that the higher number of Galerkin modes are effective only for the transient behavior. Therefore, as it was mentioned before, since the system is excited with a periodic force, and the steady state dynamic of the system is examined, the single-mode Galerkin approximation is sufficient.

The dynamical behavior of the system at point 6 is similar to the one at point 5, and as a result, the SMR occurs in this case. In addition, at point 7, the behavior of the system is similar to points 5 and 6. The only difference between the dynamical behaviors at point 7 with points 5 and 6 is the existence of the node in the slow motion phase plane for high amplitude region. The phase portrait of the slow motion of the system for parameters of point 7 is demonstrated in Figure 13.

In Figure 14, the frequency response curves of the system for point 6 are illustrated. For $-10.3 < \sigma < 16.3$ and $-10.28 < \sigma < 8.45$, the SMR and WMR occur, respectively. In Figure 15, the frequency response curves of the system for point 7 is illustrated. The range of existence of the SMR is $-14.5 < \sigma < 2.5$ in this condition. Also, The range of existence of the WMR is $-14.11 < \sigma < -5.35$ and $10.35 < \sigma < 12.1$.

The next choice of the position of the NES is at $d = 0.86$. In this case, spatial parameters of the system are $d = 0.86$, $\phi_{1o} = 1.238$ and $\phi_{1d} = 1.614$. It should be noted that in this case $\sigma = 1$ is considered. Figure 16 represents the existence of the Hopf and saddle-node bifurcations and the amplitudes of the external force for the occurrence of SMR in the $F - \alpha$

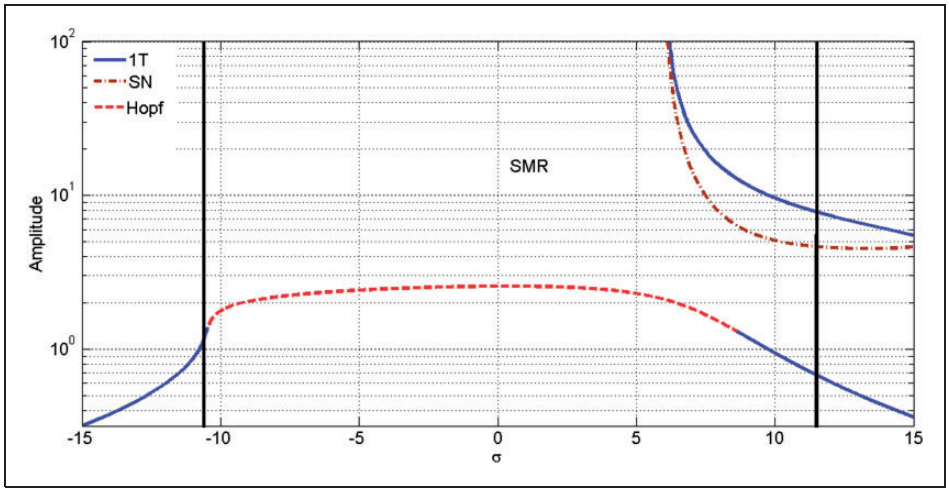

Figure 14. The Frequency response curves of the system for $d = 0.99$, $\alpha = 0.5$ and $F = 1.75$ (point 6 in Figure 6).

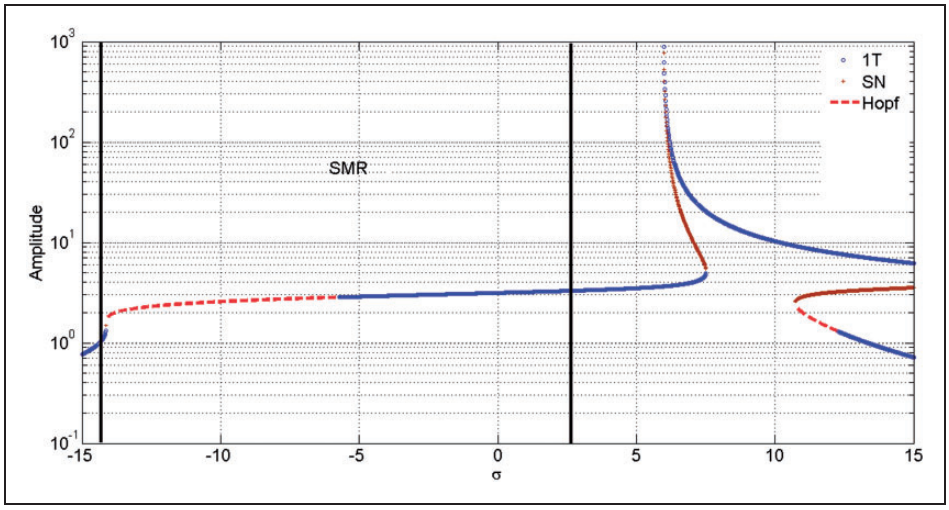

Figure 15. The Frequency response curves of the system for $d = 0.99$, $\alpha = 0.5$ and $F = 2.3$ (point 7 in Figure 6).

space. It can be seen that, the saddle node bifurcation does not occur. Furthermore, the dynamic behavior of the system at points 0, 1, 2 and 3 of Figure 16 are investigated.

As discussed in the preceding case, system with parameters of point 0 in Figure 16 has a periodic motion. Figure 17 shows the phase plane of the slow motion of the system corresponding to point 1 in Figure 16. Since in this condition the parameters of the system are located outside and lower than the Hopf bifurcation area, the node exists in the lower amplitude. In addition, there is a possibility of occurrence of the SMR. The sustained jumping map is investigated and certainty of the occurrence of SMR is approved. In Figure 18, frequency response curves of the system are depicted. The range of existence of the SMR and WMR are $-3.3 < \sigma < 2.3$ and $-3.25 < \sigma < 0.38$, respectively. It can be seen that for $\sigma = 1$, the low amplitude periodic motion and SMR exist in the system. Figure 19 shows dependency of types of the system response to various initial conditions within $-1 < q_1', \dot{q}_1', \bar{u} < 1$ and $\dot{\bar{u}} = 0$. It is shown that both types of motions occur. Of course, in most cases, in the range of the above-mentioned initial conditions, the SMR occurs. It is clear that for the lower values of initial conditions, the SMR will be less likely to occur.

The dynamical behavior of the system at point 2 is identical to those of point 1 and the SMR happens. The only difference between the dynamical behaviors at

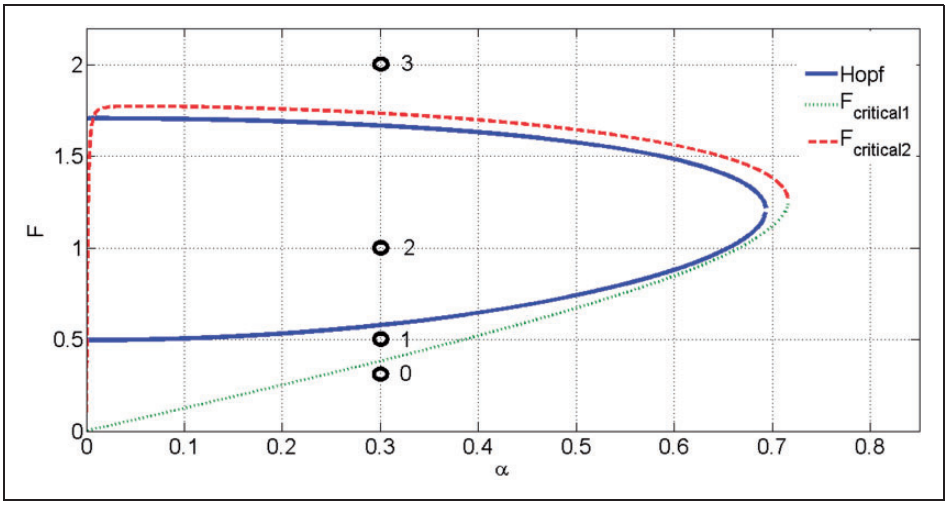

Figure 16. The occurrence of Hopf and saddle-node bifurcations, and the amplitudes of the external force for occurrence of the SMR in the $F-\alpha$ space for $\sigma = 1$ and $d = 0.86$.

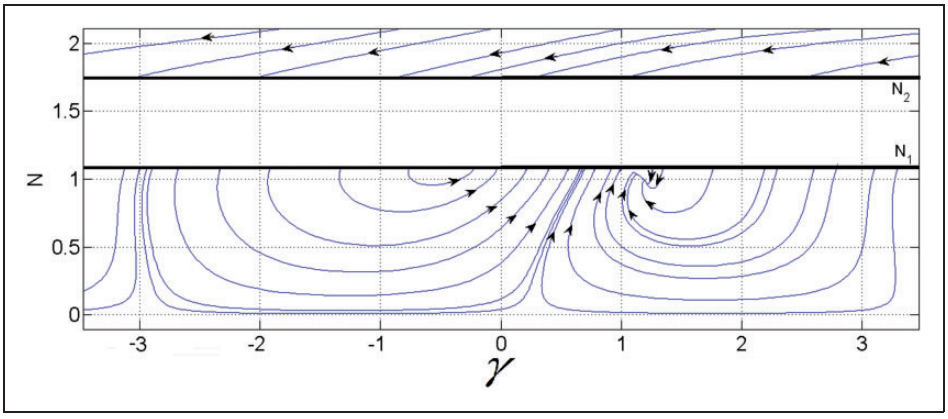

Figure 17. The phase plane of slow motion of the system for $d = 0.86$, $\sigma = 1$, $F = 0.5$ and $\alpha = 0.3$ (point 1 in Figure 16).

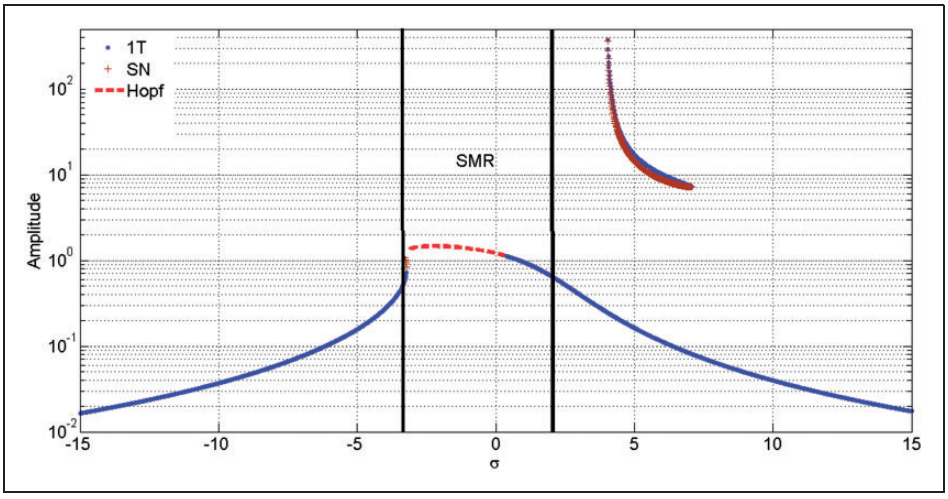

Figure 18. The frequency response curves of the system for $d = 0.86$, $\alpha = 0.3$ and $F = 0.5$ (point 1 in Figure 16).

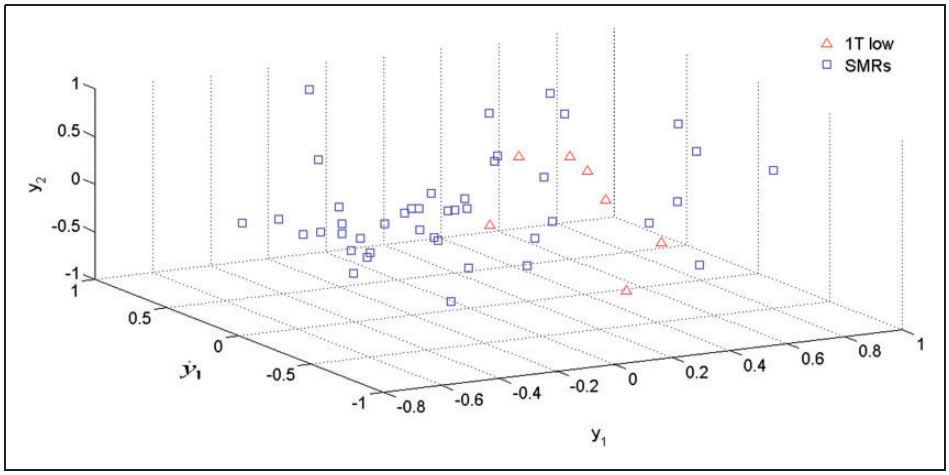

Figure 19. Dependency of the system response to initial conditions within $-1 < q_1', \dot{q}_1', \bar{u} < 1$ and $\dot{\bar{u}} = 0$ for $d = 0.86$, $\alpha = 0.3$ and $F = 0.5$ (point 1 in Figure 16) and $\sigma = 1$.

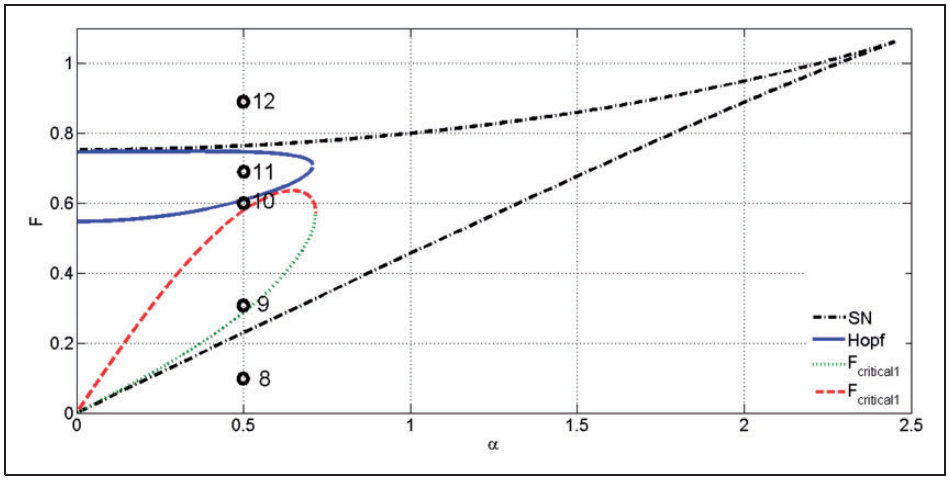

Figure 20. The existence of the Hopf and saddle-node bifurcations and the amplitudes of the external force for occurrence of the SMR in the $F - \alpha$ space for $\sigma = 1$ and $d = 0.5$.

point 2 and point 1 is the existence of node in the slow motion phase plane. Since at point 2, the parameters of the system are located inside the Hopf bifurcation area, the node does not exist in the slow motion phase plane. The range of existence of the SMR and WMR are $-6.2 < \sigma < 5.7$ and $-7.69 < \sigma < 3.7$, respectively. Also, for the parameters of point 3, the SMR occurs and the node exists in the high amplitude region of the slow motion phase plane.

The next section for the NES position is $d = 0.5$. In this case, spatial parameters of the system are $d = 0.5$, $\phi_{1o} = 2.945$, $\phi_{1d} = 0.679$ for $\sigma = 1$. Figure 20 shows the occurrence of hopf and saddle node bifurcations and the amplitudes of the external force for occurrence of SMR in the $F - \alpha$ space. It can be seen, unlike the previous cases, the saddle node bifurcation in this condition occurs for $\sigma = 1$. In this case, for points 8, 9, 10, 11 and 12 the dynamic behavior of the system is studied which is shown in Figure 20.

As previously discussed, the system with parameters of point 8 in Figure 20 has a periodic motion. The numerical results demonstrate that in comparison with the previous case, the transient response has a longer time. By studying the phase plane of the slow motion of the system related to point 9, it is clear that there is a possibility of occurrence of SMR. The sustained jumping map shows that the SMR does not occur. In Figure 21, the trajectory of the slow motion of the system in the phase plane is plotted. As it can be seen, the dynamic of the system after several motions in the closed orbit (demonstrating the SMR) is absorbed to the low amplitude node (demonstrating the low

amplitude periodic motion). For $-0.3 < \sigma < 0.9$ and $-0.33 < \sigma < 0.1$, the SMR and WMR occur, respectively.

Figure 22 shows the phase plane of the slow motion of the system related to point 10 in Figure 20. Since the parameters of system are located inside of the saddle node bifurcation area, two nodes exist in the lower and higher amplitudes, in the slow motion phase plane. Also, there is a possibility of the occurrence of SMR. The sustained jumping map is calculated and the occurrence of SMR is confirmed. The range of occurrence of the SMR and WMR in this situation are $-1.1 < \sigma < 2.1$ and $-1.215 < \sigma < 0.98$, respectively. The dynamical behavior of the system in point 11 is identical to that of point 10, and therefore, the SMR occurs. The main difference between the dynamical behaviors in points 11 and 10 is that one of two nodes in the slow motion phase plane is disappeared. Also, for the parameters of point 12, the SMR occurs and the node in the slow motion phase plane exists in the higher amplitude region.

The last section for the NES position is $d = 0.3$, which is close to the roots of the beam. In this case, spatial parameters of the system are $d = 0.3$, $\phi_{1o} = 7.327$, $\phi_{1d} = 0.273$ for $\sigma = 1$. Figure 23 depicts the occurrence of hopf and saddle-node bifurcations and amplitudes of the external force for occurrence of the SMR in the F-α space. Also, the dynamic behavior of the system is evaluated for parameters of the points 13, 14, 15, 16 and 17 in Figure 23.

The system with parameters of point 13 in Figure 23 has a periodic motion. In Figure 24, the trajectory of the slow motion of the system in the phase plane for parameters of point 14 is demonstrated. It can be seen, the system is attracted slowly to the low amplitude node. This is the sign of the longer transient response in this case. It can be explained that when the absorber is connected to the root side of the rotating beam, the

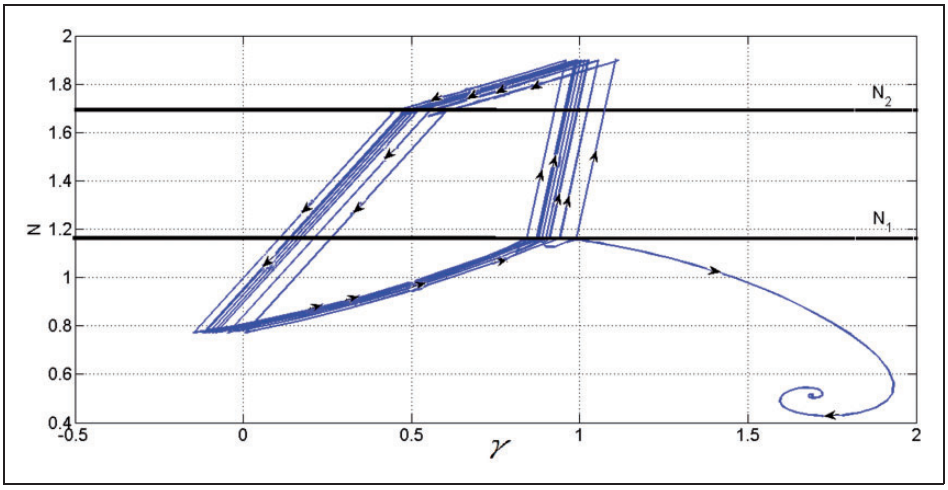

Figure 21. The trajectory of the slow motion in the phase plane for $d = 0.5$, $\sigma = 1$, $F = 0.3$ and $\alpha = 0.5$ (point 9 in Figure 20).

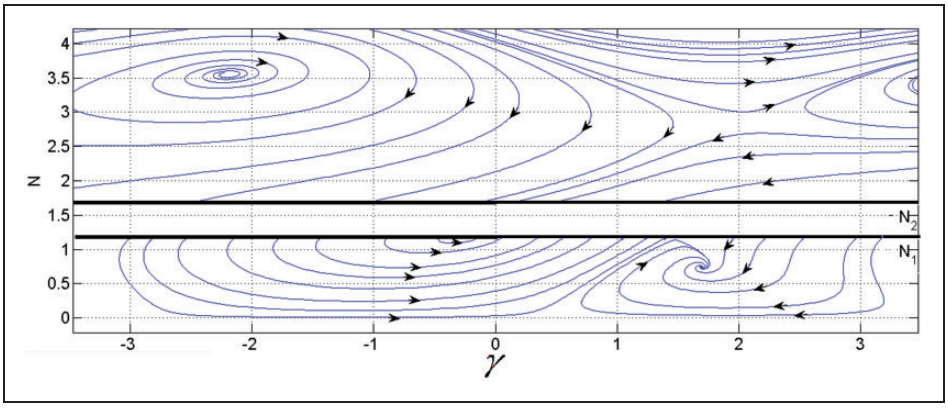

Figure 22. The Phase plane of slow motion for $d = 0.5$, $\sigma = 1$, $F = 0.6$ and $\alpha = 0.5$ (point 10 in Figure 20).

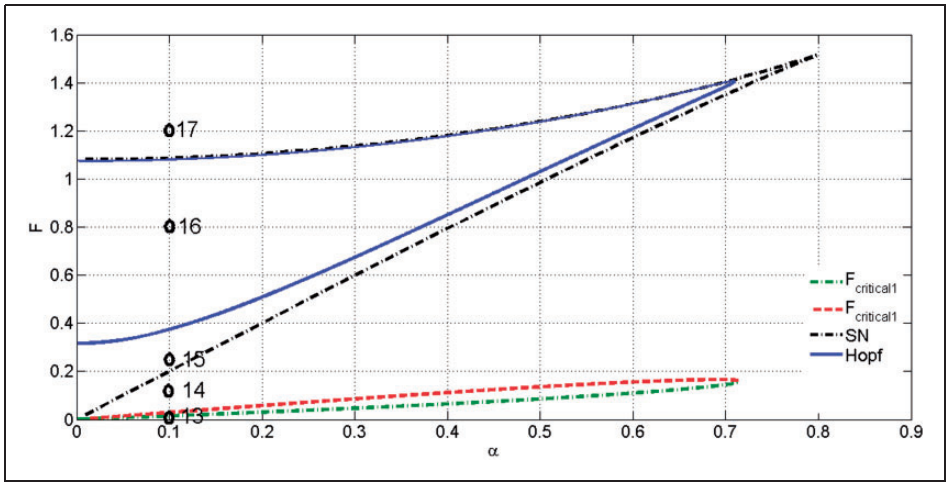

Figure 23. The existence of the Hopf and saddle-node bifurcations and the amplitudes of the external force for the occurrence of the SMR in the $F-\alpha$ space for $\sigma = 1$ and $d = 0.3$.

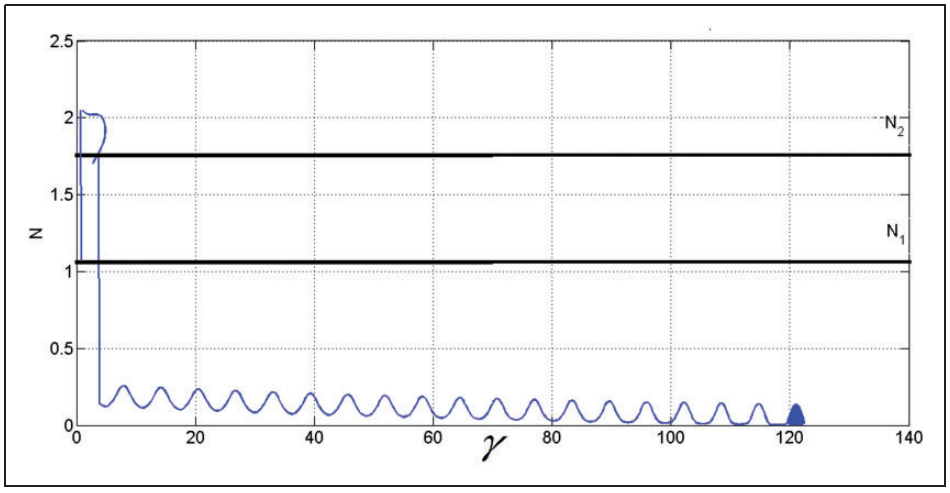

Figure 24. The trajectory of the slow motion of the system in the phase plane for $d = 0.3$, $\sigma = 1$, $F = 0.1$ and $\alpha = 0.1$ (point 14 in Figure 23).

vibration amplitude of the rotating beam is smaller at this position and as a result, absorber needs a longer time to transfer the system toward the desired motion regime. The range of the occurrence of the SMR and the WMR are $0.05 < \sigma < 0.15$ and $-0.415 < \sigma < 0.04$, respectively.

The range of existence of the SMR and WMR for parameters of point 15 are $0.05 < \sigma < 0.15$ and $-1.12 < \sigma < 0.19$, respectively. The SMR for parameters of the points 16 and 17 does not occur, at all. It can be seen, the SMR as a sign of the absorber performance, is limited and often does not occur at all in this NES position.

Finally, efficiency of the optimal NES (corresponding to point 6 in Figure 6 parameters) is compared with the optimal linear absorber. The parameters related to point 6 (in Figure 6) and around it, are selected as the optimal parameters for the NES, because in this point, the range of occurrence of the SMR in the frequency response curve is the greatest ($-10.3 < \sigma < 16.3$) in compare to other points parameters of the system. The optimal linear absorber parameters are derived from Den Hartog relation (1985). To compare these two cases, the absorbers mass and damping have the same magnitude. The absorbers stiffnesses are obtained according to the tuning of the parameters for the optimal absorbers. In addition, the amplitude and the angular frequency of the external forces for two cases have the same magnitude.

To compare the efficiency of the linear absorber and the NES in the vibration mitigation of the rotating beam, the variance of the displacement of the rotating

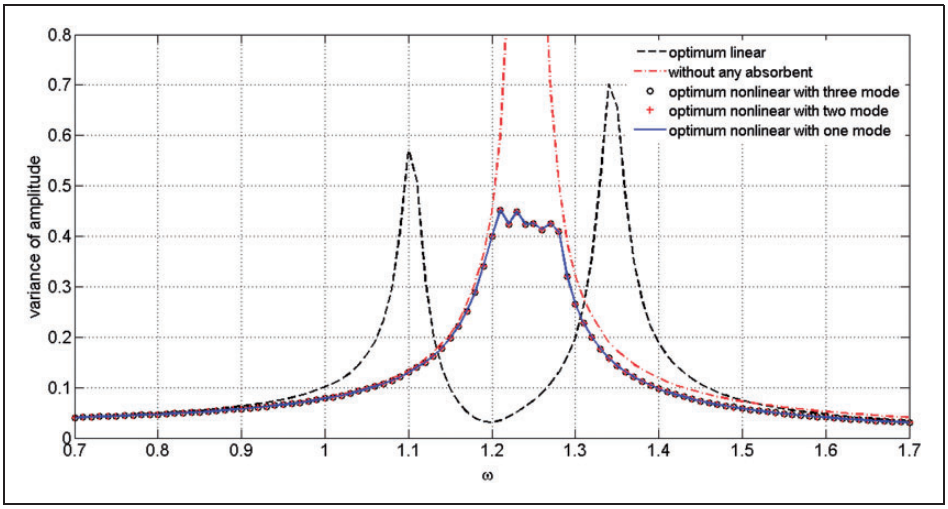

Figure 25. Thevariance of the displacement of the rotating beam without any absorber, with the optimal NES (with one, two and three first Galerkin modes of the beam), and the optimal linear absorber attached to the end of the beam ($d = 0.99$).

beam for different values of external force angular frequency, around resonance frequency is calculated.

Figure 25 shows the variance of the displacement of the rotating beam without any absorber, with attached optimal NES (one, two and three first Galerkin modes of the beam), and the attached optimal linear absorber under external force with different angular frequency (ω). Obviously, the steady state responses of the beam with attached NES are the same when considering one, two or three first Galerkin modes. As it can be seen, the linear optimal absorber right on and near the resonance frequency is more efficient than the NES. It can be seen, according to the classical properties of the linear absorbers, the resonance frequency of the system is divided into two frequencies around itself. At these frequencies, the rotating beam has a large amplitude that is an improper property of the linear absorbers. Right on and near the resonance frequency, the response of the rotating beam with the NES is non-smooth. The analytical solution demonstrates that in this region the system behavior is the SMR. Outside this region, the response of the rotating beam with the NES is smooth. The reason for this phenomenon is that the SMR does not occur and the system is attracted to a low amplitude periodic motion in this region.

In general, one can say that the optimal linear absorber is more efficient than the NES, right on and near the resonant frequency. However, in a large frequency range around the resonance frequency, the NES is more appropriate than the optimal linear absorber. When a system has a variable natural frequency or is under a variable external excitation frequency, this characteristic of the NES is significant. For example, a turbine blades may have a variant natural frequency due to erosion over time, lack of precision in manufacturing process, etc.

6. Conclusions

In this paper, the performance of a smooth NES to mitigate vibration of a rotating beam under external force is investigated. The rotating beam is modeled using the Euler-Bernoulli beam theory and the effect of centrifugal stiffening is considered. It is assumed that the nonlinear energy sink has a linear damping and an essentially nonlinear (nonlinearizable or cubic) stiffness. The conditions of occurrence of the Hopf bifurcation, saddle-node bifurcation and the SMR are investigated. The influences of position and the damping of the NES and the magnitude of external force on the vibration mitigation of the rotating beam are studied. The most important results of this paper can be represented as:

- The range of the parameters in which the SMR and the WMR occur simultaneously is the best status for attenuating purposes. In this case, the system dynamic behavior is usually attracted to the SMR that is a desirable dynamic regime.
- Also, the range of the parameters in which low amplitude periodic motion, high amplitude periodic motion, and SMR occur simultaneously is desirable, if this range is close to the occurrence range of SMR and WMR, simultaneously. In addition, in this condition, system is usually attracted to the SMR.
- Generally, for various NES positions, the SMR occurs in the middle range of the external force amplitude. Also, for different NES positions, the range of

magnitude of external force for occurrence of the SMR is different. This is one of the advantages of using NES in compare to the linear absorbers as the vibration absorber for the rotating beam.

- In general, we can say that the optimal linear absorber is more efficient than the NES, right on and near the resonant frequency. However, in the large frequency range around the resonance frequency, the NES is more appropriate.
- Occurrence of the saddle-node bifurcation has not definitive effects on the desirable behavior of the system.
- In addition, generally the appropriate range of the detuning parameter σ is negative.
- The best position of the NES is at the beam tip. When the NES position is near the root, with the best parameters of that section, the range of occurrence of SMR in the frequency response curve is smaller and transient response has a longer time. However, when the NES is attached to the outer section of the rotating beam, the range of occurrence of the SMR in the frequency response curve is greater and transient response has a shorter time. Based on these facts, the best range of the NES parameters for efficient vibration attenuation corresponds to point 6 in Figure 6.

Acknowledgements

The authors would like to thank the Energy and Control Center of Excellence of Amirkabir University of Technology of Iran for support of this research.

Conflict of interest

The authors declare no conflict of interest.

Funding

This research received no specific grant from any funding agency in the public, commercial or not-for-profit sectors.

References

Ahmadabadi ZN and Khadem SE (2012a) Self-excited oscillations attenuation of drill-string system using nonlinear energy sink. *Journal Mechanical Engineering Science* 227(2): 230–245.

Ahmadabadi ZN and Khadem SE (2012b) Annihilation of high-amplitude periodic responses of a forced two degrees of freedom oscillatory system using nonlinear energy sink. *Journal of Vibration and Control* 19: 2401–2412.

Ahmadabadi ZN and Khadem SE (2012c) Nonlinear vibration control of a cantilever beam by a nonlinear energy sink. *Mechanism and Machine Theory* 50: 134–149.

Ahmadabadi ZN and Khadem SE (2014) Nonlinear vibration control and energy harvesting of a beam using a nonlinear energy sink and a piezoelectric device. *Journal of Sound and Vibration* 333: 4444–4457.

Bab S, Khadem SE and Shahgholi M (2014) Vibration mitigation of a rotor supported by journal bearings with nonlinear suspensions under mass eccentricity force using nonlinear energy sink. *International Journal of Non-Linear Mechanics* 67: 251–266.

Byers L and Gandhi F (2009) Embedded absorbers for helicopter rotor lag damping. *Journal of Sound and Vibration* 325: 705–721.

Dai X, Shen Z and Wei H (2001) On the vibration of rotor-bearing system with squeeze film damper in an energy storage flywheel. *International Journal of Mechanical Sciences* 43: 2525–2540.

Den Hartog JP (1985) *Mechanical Vibrations*. New York: Dover Publications.

Domany E and Gendelman OV (2013) Dynamic responses and mitigation of limit cycle oscillations in Van der Pol–Duffing oscillator with nonlinear energy sink. *Journal of Sound and Vibration* 332: 5489–5507.

Duffy CP, Bagley RL and Mehmed O (2000) On a Self-Tuning Impact Vibration Damper for Rotating Turbomachinery. In: *Joint Propulsion Conference*, Huntsville, Alabama.

Duffy CP, Brown GV and Bagley RL (2004) Self-tuning impact damper for rotating blades. *United States Patent*, US 6,827,551 B1.

Ewins DJ (2010) Control of vibration and resonance in aero engines and rotating machinery- an overview. *International Journal of Pressure Vessels and Piping* 87-9: 504–510.

Fenichel N (2006) Persistence and smoothness of invariant manifolds for flows. *Indiana Univ. Math. J* 21: 193–225.

Gendelman OV (2004) Bifurcations of Nonlinear Normal Modes of Linear Oscillator with Strongly Nonlinear Damped Attachment. *Nonlinear Dynamics* 37: 115–128.

Gendelman OV (2008) Targeted energy transfer in systems with non-polynomial nonlinearity. *Journal of Sound and Vibration* 315: 732–745.

Gendelman OV (2011) Targeted energy transfer in systems with external and self-excitation. *Proceedings of the Institution of Mechanical Engineers, Part C: Journal of Mechanical Engineering Science* 225: 2007–2043.

Gendelman OV, Starosvetsky Y and Feldman M (2008) Attractors of harmonically forced linear oscillator with attached nonlinear energy sink I: description of response regimes. *Nonlinear Dynamics* 51: 31–46.

Genta G (2005) *Dynamics of Rotating Systems*. New York: Springer.

Georgiades F and Vakakis AF (2007) Dynamics of a linear beam with an attached local nonlinear energy sink. *Communications in Nonlinear Science and Numerical Simulation* 12: 643–651.

Georgiades F and Vakakis AF (2009) Passive targeted energy transfers and strong modal interactions in the dynamics of a thin plate with strongly nonlinear attachments. *International Journal of Solids and Structures* 46: 2330–2353.

Georgiades F, Vakakis AF and Kerschen G (2007) Broadband passive targeted energy pumping from a linear dispersive rod to a lightweight essentially nonlinear end attachment. *International Journal of Non-Linear Mechanics* 42: 773–788.

Gerges R and Vickery BJ (2003) Wind tunnel study of the across-wind response of a slender tower with a nonlinear tuned mass damper. *Journal of Wind Engineering and Industrial Aerodynamics* 91: 1069–1092.

Grinberg I, Lanton V and Gendelman OV (2012) Response regimes in linear oscillator with 2DOF nonlinear energy sink under periodic forcing. *Nonlinear Dynamics* 69: 1889–1902.

Lamarque CH, Gendelman OV, Savadkoohi AT and Etcheverria E (2011) Targeted energy transfer in mechanical systems by means of non-smooth nonlinear energy sink. *Acta Mechanica* 221: 175–200.

Lamarque CH and Savadkoohi AT (2014a) Dynamical behavior of a Bouc–Wen type oscillator coupled to a nonlinear energy sink. *Meccanica* 49: 1917–1928.

Lamarque CH and Savadkoohi AT (in press) Targeted energy transfer between a system with a set of Saint-Venant elements and a nonlinear energy sink. *Continuum Mechanics and Thermodynamics* DOI 10.1007/s00161 014-0354-9.

Lee YS, Vakakis AF, Bergman LA and McFarland DM (2006) Suppression of limit cycle oscillations in the van der Pol oscillator by means of passive non-linear energy sinks. *Structural Control Health Monitoring* 13: 41–75.

Lee YS, Vakakis AF, Bergman LA, McFarland DM and Kerschen G (2007) Suppressing Aeroelastic Instability Using Broadband Passive Targeted Energy Transfers, Part 1: Theory. *AIAA Journal* 45: 693–711.

Luongo A and Zulli D (2012) Dynamic analysis of externally excited NES-controlled systems via a mixed Multiple Scale/Harmonic Balance algorithm. *Nonlinear Dynamic* 70: 2049–2061.

Luongo A and Zulli D (2013) Aeroelastic instability analysis of NES-controlled systems via a mixed multiple scale/harmonic balance method. *Journal of Vibration and Control* 20(13): 1985–1998.

Manevitch L (2001) The description of localized normal modes in a chain of nonlinear coupled oscillators using complex variables. *Nonlinear Dynamic* 25: 95–109.

Manevitch AI and Manevitch L (2005) *The Mechanics of Nonlinear systems with Internal Resonances*. London: Imperial College Press London.

Mehmood A, Nayfeh AH and Hajj MR (2014) Effects of a non-linear energy sink (NES) on vortex-induced vibrations of a circular cylinder. *Nonlinear Dynamics* 77: 667–680.

Meirovitch L (2001) *Fundamentals of Vibrations*. New York: McGraw Hill.

Nayfeh AH and Balachandran B (2004) *Applied Nonlinear Dynamics*. New York: Wiley-Interscience.

Samani FS and Pellicano F (2009) Vibration reduction on beams subjected to moving loads using linear and nonlinear dynamic absorbers. *Journal of Sound and Vibration* 325: 742–754.

Sanches L, Michon G, Berlioz A and Alazard D (2011) Instability zones for isotropic and anisotropic multibladed rotor configurations. *Mechanism and Machine Theory* 46: 1054–1065.

Savadkoohi AT, Lamarque CH and Dimitrijevic Z (2012) Vibratory energy exchange between a linear and a nonsmooth system in the presence of the gravity. *Nonlinear Dynamics* 70: 1473–1483.

Starosvetsky Y and Gendelman OV (2008a) Attractors of harmonically forced linear oscillator with attached nonlinear energy sink II: optimization of a nonlinear vibration absorber. *Nonlinear Dynamics* 51: 47–57.

Starosvetsky Y and Gendelman OV (2008b) Dynamics of a strongly nonlinear vibration absorber coupled to a harmonically excited two-degree-of-freedom system. *Journal of Sound and Vibration* 312: 234–256.

Vakakis AF, Gendelman O, Bergman LA, McFarland DM, Kerschen G and Lee YS (2008) *Passive Nonlinear Targeted Energy Transfer in Mechanical and Structural Systems: I and II*. New York: Springer Verlag.

Vaurigaud B, Manevitch LI and Lamarque CH (2013) Suppressing Aeroelastic Instability in a Suspension Bridge Using a Nonlinear Absorber. *IUTAM Symposium on Nonlinear Dynamics for Advanced Technologies and Engineering Design* 32: 263–277.

Weiss M, Savadkoohi AT, Gendelman OV and Lamarque CH (2014) Dynamical behavior of a mechanical system including Saint-Venant component coupled to a nonlinear energy sink. *International Journal of Non-Linear Mechanics* 63: 10–18.

Zulli D and Luongo A (2014) Nonlinear energy sink to control vibrations of an internally nonresonant elastic string. *Meccanica* 50(3): 781–794.

Appendix

Appendix A

$$m_{11} = \int_{\bar{r}_i}^{\bar{r}_i+1} \phi_1^2(\bar{r})\mathrm{d}\bar{r},$$

$$k_{11} = \int_{\bar{r}_i}^{\bar{r}_i+1} \left(-\bar{\Omega}^2\phi_1^2(\bar{r}) + \bar{\Omega}^2\bar{r}\phi_1(\bar{r})\frac{d\phi_1(\bar{r})}{\mathrm{d}\bar{r}} - \phi_1(\bar{r})\frac{\bar{\Omega}^2}{2}(\bar{r}_0^2 - \bar{r}^2) + \phi_1(\bar{r})\frac{\mathrm{d}^4\phi_1(\bar{r})}{\mathrm{d}\bar{r}^4}\right)\mathrm{d}\bar{r}$$

Appendix B

$$\gamma_1 = \alpha(1 + \varepsilon\phi_{1d}^2),$$

$$\gamma_2 = \frac{1}{64\omega_0^6}\{16\bar{\omega}^6\alpha^2 - 48\bar{\omega}^4\beta\phi_{20}^2 + 27\beta^2\phi_{20}^4 + 16\varepsilon^2\sigma^2\bar{\omega}^4 + 32\bar{\omega}^6\alpha^2\varepsilon\phi_{1d}^2 + 16\bar{\omega}^6\varepsilon^2\alpha^2\phi_{1d}^4 + 54\beta^2\phi_{20}^4\varepsilon\phi_{1d}^2 + 27\varepsilon^2\beta^2\phi_{20}^4\phi_{1d}^4 + 16\bar{\omega}^8 + 48\bar{\omega}^2\varepsilon^2\sigma\beta\phi_{20}^2\phi_{1d}^2\},$$

$$\gamma_3 = \frac{\bar{\omega}^{10}\varepsilon\alpha\phi_{1d}^2 + \sigma^2\varepsilon^2\alpha\bar{\omega}^6}{4\bar{\omega}^8},$$

$$\gamma_4 = \frac{\varepsilon^2}{256\bar{\omega}^8}\{16\sigma^2\bar{\omega}^8 + 16\sigma^2\alpha^2\bar{\omega}^6 + 27\sigma^2\beta^2\phi_{20}^4 + 48\sigma\bar{\omega}^6\beta\phi_{20}^2\phi_{1d}^2 - 54\bar{\omega}^2\sigma\beta^2\phi_{20}^4\phi_{1d}^2 + 27\bar{\omega}^4\beta^2\phi_{20}^4\phi_{1d}^4 - 32\sigma\bar{\omega}^8\alpha^2\phi_{1d}^2 - 48\sigma^2\beta\phi_{20}^2\bar{\omega}^4 + 16\bar{\omega}^{10}\alpha^2\phi_{1d}^2\}$$

Appendix C

$$
\begin{aligned}
v_1 = &-\frac{27}{128}\frac{\alpha^2\varepsilon^4\phi_{1d}^6\sigma\beta^2}{\bar{\omega}^6}-\frac{27}{128}\frac{\alpha^2\varepsilon^2\phi_{1d}^2\sigma\beta^2}{\bar{\omega}^6}\\
&-\frac{27}{64}\frac{\alpha^2\varepsilon^3\phi_{1d}^4\sigma\beta^2}{\bar{\omega}^6}-\frac{27}{128}\frac{\alpha^2\varepsilon^4\phi_{1d}^4\beta^2\sigma^2}{\bar{\omega}^8}\\
&-\frac{27}{256}\frac{\alpha^2\varepsilon^5\phi_{1d}^6\beta^2\sigma^2}{\bar{\omega}^8}-\frac{27}{256}\frac{\alpha^2\varepsilon^3\phi_{1d}^2\sigma^2\beta^2}{\bar{\omega}^8}\\
&-\frac{27}{256}\frac{\alpha^2\varepsilon\phi_{1d}^2\beta^2}{\bar{\omega}^4}-\frac{27}{256}\frac{\alpha^2\varepsilon^3\phi_{1d}^6\beta^2}{\bar{\omega}^4}-\frac{27}{128}\frac{\alpha^2\varepsilon^2\phi_{1d}^4\beta^2}{\bar{\omega}^4}\\
v_2 = &-\frac{3}{16}\frac{\alpha^2\varepsilon^5\phi_{1d}^4\sigma^3\beta}{\bar{\omega}^6}+\frac{3}{16}\frac{\alpha^2\varepsilon^2\phi_{1d}^2\sigma\beta}{\bar{\omega}^2}\\
&-\frac{3}{16}\frac{\alpha^2\varepsilon^4\phi_{1d}^4\sigma^2\beta}{\bar{\omega}^4}-\frac{3}{16}\frac{\alpha^2\varepsilon^4\phi_{1d}^4\sigma^3\beta}{\bar{\omega}^6}\\
&-\frac{3}{16}\frac{\alpha^2\varepsilon^3\phi_{1d}^2\sigma^2\beta}{\bar{\omega}^4}+\frac{3}{16}\frac{\alpha^2\varepsilon^3\phi_{1d}^4\sigma\beta}{\bar{\omega}^2}\\
&+\frac{3}{16}\alpha^2\varepsilon\phi_{1d}^2\beta+\frac{3}{16}\alpha^2\varepsilon^2\phi_{1d}^2\beta\\
v_3 = &-\frac{1}{8}\alpha^4\varepsilon^2\phi_{1d}^4\bar{\omega}^2-\frac{1}{16}\alpha^4\varepsilon^3\phi_{1d}^6\bar{\omega}^2\\
&-\frac{1}{16}\alpha^2\varepsilon\phi_{1d}^2\bar{\omega}^4-\frac{1}{16}\alpha^4\varepsilon\phi_{1d}^2\bar{\omega}^2-\frac{1}{16}\frac{\alpha^2\varepsilon^5\phi_{1d}^2\sigma^4}{\bar{\omega}^4}\\
&+\frac{1}{8}\alpha^2\varepsilon^3\phi_{1d}^2\sigma^2-\frac{1}{16}\frac{\alpha^4\varepsilon^3\phi_{1d}^2\sigma^2}{\bar{\omega}^2}-\frac{1}{16}\alpha^4\varepsilon^3\phi_{1d}^4\sigma\\
&-\frac{1}{8}\frac{\alpha^4\varepsilon^4\phi_{1d}^4\sigma^2}{\bar{\omega}^2}-\frac{1}{16}\frac{\alpha^4\varepsilon^5\phi_{1d}^6\sigma^2}{\bar{\omega}^2}\\
&-\frac{1}{8}\alpha^4\varepsilon^2\phi_{1d}^2\sigma-\frac{1}{8}\alpha^4\varepsilon^4\phi_{1d}^6\sigma
\end{aligned}
$$

Appendix D (notation)

d	The distance of the NES position from the root of the rotating beam
m, C, λ	The mass, nonlinearizable (cubic) stiffness and damping of the NES, respectively
$q_1(\bar{t})$	The displacement of the first mode of the rotating beam
$q_1'(\bar{t})$	The displacement of the first mode of the rotating beam at the NES position
r_i, r_o	The inner and outer radiuses of the rotating beam
$u(t)$, $v(r,t)$	The displacement of NES and rotating beam, respectively
$v(t)$	The displacement of the center of mass of the beam and the NES
$w(t)$	The NES displacement relative to the beam
F, ω	The amplitude and the angular frequency of the external force
$N(\tau_1)-\gamma(\tau_1)$	The amplitude and phase of the slow motion of the NES displacement relative to the beam, respectively
$O(\varepsilon)$	Order of magnitude of ε
$\delta_1(t)$, $\delta_2(t)$	The small complex quantities of perturbation around the equilibrium point φ_{10} and φ_{20}, respectively
ε	Small parameter
$\phi_j(\bar{r})$	The linear mode shapes of the rotating beam
$\phi_k(t)$, $k=1,2$	slow-varying, complex-valued amplitude modulations
ρ, A, l	The mass density, cross sectional area and length of the rotating beam
σ	The detuning parameter
$\tau_r=\varepsilon^r t$, $r=0,1,\ldots,$	The time scales
ω_1	The first natural frequency of the rotating beam
Ω	The angular velocity of the rotating beam